*J. Fluid Mech.* (2003), *vol.* 476, *pp.* 179–211.  
DOI: 10.1017/S0022112002002872 Printed in the United Kingdom

# Direct initiation of detonation with a multi-step reaction scheme

By HOI DICK NG AND JOHN H. S. LEE

Department of Mechanical Engineering, McGill University, 817 Sherbrooke Street West, Montreal, Quebec, Canada H3A 2K6

(Received 28 January 2001 and in revised form 15 August 2002)

The problem of direct initiation of detonation, where a powerful ignition source drives a blast wave into a gaseous combustible mixture to generate a Chapman–Jouguet (CJ) detonation, is investigated numerically by using a three-step chain-branching chemical kinetic model. The reaction scheme consists sequentially of a chain-initiation and a chain-branching step, followed by a temperature-independent chain termination. The three regimes of direct initiation i.e. subcritical, critical and supercritical, are numerically simulated for planar, cylindrical and spherical geometries using the present three-step chemical kinetic model. It is shown that the use of a more detailed reaction mechanism allows a well-defined value for the critical initiation energy to be determined. The numerical results demonstrate that detonation instability plays an important role in the initiation process. The effect of curvature for cylindrical and spherical geometries has been found to enhance the instability of the detonation wave and thus influence the initiation process. The results of these simulations are also used to provide further verification of some existing theories of direct initiation of detonation. It appears that these theories are satisfactory only for stable detonation waves and start to break down for highly unstable detonations because they are based on simple blast wave theory and do not include a parameter to model the detonation instability. This study suggests that a stability parameter, such as the ratio between the induction and reaction length, should be considered and a more complex chemistry should be included in future development of a more rigorous theory for direct initiation of detonation.

## 1. Introduction

Direct initiation of detonation, as opposed to the transition from deflagration to detonation, refers to the 'instantaneous' formation of a detonation in the decay of the strong blast wave ensued from a powerful ignition source. Since the pioneering work of Zel'dovich, Kogarko & Simonov (1957), significant advances have been made toward the understanding of the direct initiation phenomenon. Numerous studies were carried out which attempted to formulate a predictive theory for the critical initiation energy (see, for example, Lee 1977). In spite of all these efforts, a quantitative theory capable of predicting the critical initiation energy from first principles based on thermo-chemical and kinetic rate data of the mixture is still lacking. The weakest part of most previous theoretical and numerical investigations is the use of an idealized single-step Arrhenius rate law to model the chemical reaction kinetics. Although the use of such a model simplifies the analysis and reveals some interesting global features of the phenomenon, it does not represent effectively the chemical reactions of

most explosive mixtures. Hence, some results obtained by using a one-step chemistry model may not even be in qualitative agreement with experimental observations. For instance, in the numerical study by Mazaheri (1997), it is demonstrated that the use of a single-step Arrhenius rate law results in difficulty in obtaining a well-defined value of critical initiation energy. For single-step chemistry, a system without losses will always react to completion. Hence initiation will always occur after a sufficiently long time and a critical value of initiation energy no longer exists. This then yields the non-physical result that a detonation can be initiated via any arbitrary strength of shock wave if one waits long enough.

Numerous studies have revealed that complexities in the chemistry model are significant in the initiation and propagation of the detonation wave, as well as the detonation structure. For instance, von Neumann (1942), and more recently Sharpe (1999), Sharpe & Falle (2000) and Dionne (2000) pointed out that pathological detonations, i.e. detonations that can travel at a velocity greater than the Chapman–Jouguet (CJ) value, are possible when the chemical kinetic mechanism involves a competition between exothermic and endothermic reactions. Such non-ideal detonation usually arises due to the effects of chemistry such as the present of an endothermic stage of the reaction, mole changes during the reaction, multiple reversible reactions, etc. (see Fickett & Davis 1979).

To study the influence of chemical kinetics, Dold & Kapila (1991) investigated the difference between shock initiation of detonation based on an asymptotic analysis for global one-step and three-step chain-branching chemical models. They found that the development of the detonation behind an initiating shock wave is fundamentally different when the chemistry is modelled using a radical chain-branching mechanism from that when using a global one-step model. Their analyses indicated that a simplified one-step chemical model may not be adequate for the study of detonation initiation in combustible mixtures, which are typically burned by way of a radical chain-branching process.

Subsequently, Short & Dold (1996) conducted linear stability studies of a detonation wave using the same chain-branching reaction model as Dold & Kapila (1991). In parallel with the linear stability analyses, Short & Quirk (1997) carried out direct numerical simulations to investigate the nonlinear pulsating detonation instability driven by the three-step chain-branching reaction. They showed similar mechanisms for the regular and irregular modes of instability for both the simple one-step Arrhenius reaction and the three-step chain-branching reaction models. However, they found that the use of the three-step chain-branching reaction scheme has an advantage over the standard one-step Arrhenius model because a well-defined detonability limit can now be obtained. More recently, the dynamics of one-dimensional overdriven detonations with branched-chain kinetics has been revisited by Sánchez *et al.* (2001), providing further analytical developments of the problem.

In view of the different qualitative features obtained from these studies where a more detailed chemical kinetics is used, it appears of interest to investigate the direct blast initiation problem by including more detailed chemistry. Theoretical and numerical investigations of the blast initiation problem have already been carried out by many researchers, for instance He & Clavin (1994), Mazaheri (1997) and more recently by Eckett, Quirk & Shepherd (2000), all using a single-step Arrhenius rate law. Although He (1996) also incorporated detailed kinetics of the $H_2$–$O_2$ system in their numerical calculations, little attention is given on the influence of the chemical kinetics. Therefore, the main objective of this paper is to elucidate further the direct initiation phenomenon and investigate the importance of the chemical kinetic scheme used. The

present investigation is carried out via numerical simulations. A number of numerical schemes are nowadays available which are capable of reproducing many aspects of the highly transient and unstable events during the initiation and propagation of gaseous detonations (see Bourlioux, Majda & Roytburd 1991). Numerical simulations can provide more detailed information on the non-steady reacting flow field behind the detonation, which can be difficult to obtain from experiments. Although a complex set of chemical kinetic rate equations could in principle be solved simultaneously with the reactive Euler equations within current computational capabilities, interpretation of the large amount of detailed information generated by such numerical simulations becomes a challenging problem. Therefore, it may suffice to use a simplified chemical kinetics of the three-step reaction mechanism to just more accurately reproduce some qualitative aspects of the initiation phenomenon. In the present study, the same three-step chain-branching reaction model as in the work of Short & Quirk (1997) is used to simulate the direct initiation phenomenon. This model consists of a chain-initiation and a chain-branching step, followed by a temperature-independent chain termination. It can represent a generic three-step chemical-kinetic description of a real chain-branching reaction.

## 2. Mathematical model

The dynamics of unsteady propagation of a one-dimensional detonation can be described by the one-dimensional reactive Euler equations, i.e. a set of hyperbolic partial differential equations in space (in laboratory frame) and time that express the conservation of mass, momentum and energy. They have the following non-dimensional form:

$$\frac{\partial \rho}{\partial t} + \frac{\partial (\rho u)}{\partial r} + \frac{j}{r}(\rho u) = 0, \tag{2.1a}$$

$$\frac{\partial (\rho u)}{\partial t} + \frac{\partial}{\partial r}(\rho u^2 + p) + \frac{j}{r}(\rho u^2) = 0, \tag{2.1b}$$

$$\frac{\partial (\rho e)}{\partial t} + \frac{\partial}{\partial r}[u(\rho e + p)] + \frac{j}{r}[u(\rho e + p)] = 0, \tag{2.1c}$$

where $\rho$, $u$, $p$ and $e$ denote the fluid density, velocity, pressure and specific total energy, respectively. The parameter $j$ represents the geometric factor with $j = 0$, 1, 2 for the planar, cylindrical and spherical geometries. Assuming a perfect gas with constant specific heat ratio $\gamma$, the specific total energy and the equation of state are given by

$$e = \frac{p}{(\gamma - 1)\rho} - q + \tfrac{1}{2}u^2, \tag{2.2a}$$

$$p = \rho T, \tag{2.2b}$$

where $q$ is the local chemical energy release. All the flow variables are non-dimensionalized with respect to the unburned mixture properties as follows:

$$\rho = \frac{\tilde{\rho}}{\tilde{\rho}_o}, \quad p = \frac{\tilde{p}}{\gamma \tilde{p}_o}, \quad T = \frac{\tilde{T}}{\gamma \tilde{T}_o}, \quad u = \frac{\tilde{u}}{\tilde{c}_o},$$
$$E_a = \frac{\tilde{E}_a}{\tilde{c}_o^2}, \quad Q = \frac{\tilde{Q}}{\tilde{c}_o^2} \quad \text{with} \quad \tilde{c}_o^2 = \frac{\gamma \tilde{p}_o}{\tilde{\rho}_o}, \tag{2.3}$$

where we use the tilde to denote dimensional quantities and subscript ($o$) to denote quantities ahead of the shock. The variable $\tilde{c}_o$ is the sound speed of the unburned mixture. The reference length and time scales will be described later in this section.

The chemical kinetic model used for the present study is a generalized three-step chain-branching reaction model and its detailed description can be found in the paper by Short & Quirk (1997). For completeness, we will just summarize its main features here. This model involves two temperature-sensitive radical-producing reactions and a temperature-independent chain-termination reaction. It can be represented by the following three main stages:

1. Chain initiation: $F \rightarrow Y$, $\quad k_I = \exp\left(E_I\left(\frac{1}{T_I} - \frac{1}{T}\right)\right)$, (2.4*a*)

2. Chain branching: $F + Y \rightarrow 2Y$, $\quad k_B = \exp\left(E_B\left(\frac{1}{T_B} - \frac{1}{T}\right)\right)$, (2.4*b*)

3. Chain termination: $Y \rightarrow P$, $\quad k_C = 1$, (2.4*c*)

where $F$, $Y$ and $P$ correspond to the amount of reactant, radical and product, respectively. The chain-initiation and chain-branching rate constants $k_I$ and $k_B$ have an Arrhenius temperature-dependent form $\mathrm{e}^{-E/T}$. The chain-termination reaction is assumed to be first order, independent of temperature and to have a fixed rate constant $k_C$. The initiation step has the activation energy $E_I$ and the activation energy for the chain-branching step is $E_B$. The parameters $T_I$ and $T_B$ denote respectively the chain-initiation and chain-branching cross-over temperatures. These are the temperature limits at which the chain-initiation and chain-branching rates become as fast as the chain-termination rate. In order to represent typical chain-branching reactions, these parameters should lie within the following limits (Short & Quirk 1997):

$$T_I > T_{shock}, \quad T_B < T_{shock}, \quad E_I \gg E_B. \tag{2.5}$$

The reference length scale $\tilde{r}_c$ is chosen such that the chain-termination rate constant is unity, i.e. $k_C = 1$. The reference time scale $\tilde{t}_c$ is therefore set to the reference length scale divided by the sound speed of the reactant (i.e. $\tilde{t}_c = \tilde{r}_c/\tilde{c}_o$). Denoting the variables $f$ and $y$ to be the mass fraction of the fuel $F$ and radical $Y$, the consumption equations for fuel and radical can be written as

$$\frac{\partial(\rho f)}{\partial t} + \frac{\partial(\rho u f)}{\partial r} + \frac{j}{r}(\rho u f) = -\rho(w_I + w_B), \tag{2.6a}$$

$$\frac{\partial(\rho y)}{\partial t} + \frac{\partial(\rho u y)}{\partial r} + \frac{j}{r}(\rho u y) = \rho(w_I + w_B - w_C), \tag{2.6b}$$

where

$$w_I = f\exp\left(E_I\left(\frac{1}{T_I} - \frac{1}{T}\right)\right), \quad w_B = \rho f y \exp\left(E_B\left(\frac{1}{T_B} - \frac{1}{T}\right)\right), \quad w_C = y, \tag{2.7}$$

and the local chemical energy release is given by

$$q = Q - fQ - y(Q + Q_{endo}), \tag{2.8}$$

where $Q$ is the total amount of chemical energy available in the combustible mixture and $Q_{endo}$ represents the amount of endothermic chemical energy used by the chain-initiation and chain-branching reactions because energy is required to break the bond and dissociate the reactant into free radicals. In the present work, $Q_{endo}$ is set to zero for simplicity without loss of generality. The three-step chemical kinetic model allows four parameters to be adjusted, namely $E_I$, $E_B$, $T_I$ and $T_B$. It should be noted that it is possible to derive a number of different steady detonation profiles under the

ordered limits allowed by these parameters (Short, Kapila & Quirk 1999). This model has an advantage over the standard single-step chemistry model because it allows the variation of the two important length scales of the reaction process, namely the induction and reaction zone length. In the present study, values of $Q = 8.33$, $E_I = 37.5$, $E_B = 10$, $T_I = 3T_{shock}$ and $\gamma = 1.2$ are used throughout for the CJ detonation, unless specified otherwise. The chain-branching cross-over temperature $T_B$ is also used as a bifurcation parameter.

## 3. Detonation structure

### 3.1. *Steady-state ZND structure*

Before we investigate the dependence of the direct initiation process on the details of the chemistry model, it is worthwhile to first obtain the steady ZND (Zel'dovich–von Neumann–Döring) detonation structure using the generalized three-step chemical kinetic model. The variation of the state variables in the detonation structure can be obtained via the integration of the three conservation equations together with the chemical rate law. The non-dimensional steady-state conservation equations for a coordinate system fixed with respect to the shock front can be written as

$$M = \frac{u}{v}, \tag{3.1a}$$

$$\frac{1}{\gamma} + M^2 = p + \frac{u^2}{v} = p + Mu, \tag{3.1b}$$

$$\frac{1}{\gamma - 1} + \frac{M^2}{2} = \frac{\gamma pv}{\gamma - 1} + \frac{u^2}{2} - (Q - fQ - yQ), \tag{3.1c}$$

where $M$ is the Mach number of the CJ detonation wave and $v$ the specific volume (i.e. $1/\rho$). The variation in fuel and radical concentrations is determined by the following equations:

$$f_r = -(w_I + w_B)/u, \quad y_r = (w_I + w_B - w_C)/u, \tag{3.2}$$

where the subscript $r$ denotes the derivative with respect to the distance $r$ and $w$ represents the rate of each reaction step as given previously by equations (2.7). The above system of equations can be integrated using the initial condition of the shocked state (or von Neumann state). For a given shock Mach number, the von Neumann state can be obtained from the Rankine–Hugoniot relationship for a normal shock wave. The integration proceeds until the equilibrium CJ conditions are reached.

Typical pressure and temperature profiles for the ZND structure are illustrated in figure 1($a, b$). Across the shock, the pressure and temperature jump abruptly to the von Neumann state. During the induction period both the pressure and temperature remain relatively constant. When energy starts to be released in the reaction zone, the pressure drops while the temperature increases. At the end of the reaction zone, the products are at equilibrium and the final state corresponds to values from the CJ solution, if the unique CJ detonation velocity (at which the equilibrium or burnt zone flow is sonic relative to the shock front) is used. From figure 1, two distinct regions can be clearly recognized after the shock front: a induction zone and a reaction zone. In the induction zone where the 'incubation' process occurs, the reactants start to dissociate into free radicals. The free radicals then participate in the exothermic recombination process when the chemical energy is released and temperature increases.

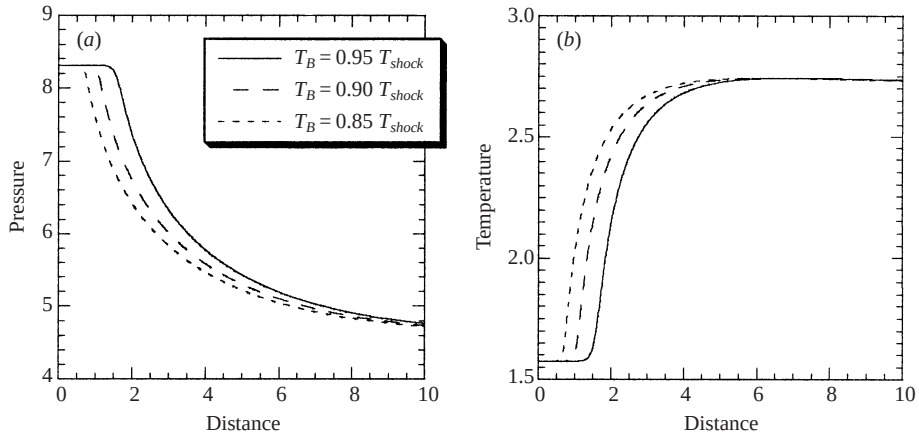


FIGURE 1. Steady ZND detonation profiles for a mixture with $Q = 8.33$, $\gamma = 1.2$, $E_I = 37.5$, $E_B = 10$ and $T_I = 3T_{shock}$. (*a*) Pressure profile; (*b*) temperature profile.

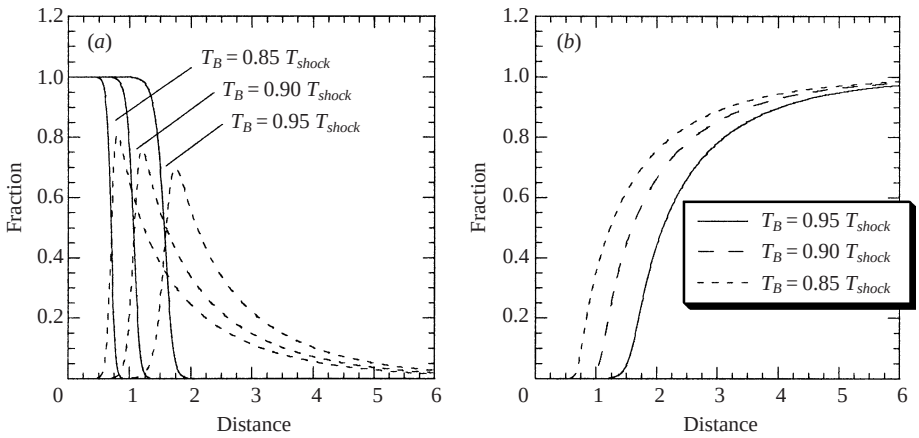


FIGURE 2. Steady ZND detonation profiles for a mixture with $Q = 8.33$, $\gamma = 1.2$, $E_I = 37.5$, $E_B = 10$ and $T_I = 3T_{shock}$. (*a*) Mass fraction of fuel (solid line) and radical (dashed line); (*b*) mass fraction of product.

It is also demonstrated that the chain-branching cross-over temperature $T_B$ controls the ratio of the induction length to the recombination length (Short & Quirk 1997). In figures 1(*a*) and 1(*b*), $T_B$ varies from $0.85T_{shock}$ to $0.95T_{shock}$ while the other parameters are held constant. By increasing parameter $T_B$, the induction zone length increases relative to the recombination zone. This is shown more clearly if we look at the profiles for the consumption of reactant as well as the formation of product.

Figure 2(*a*, *b*) shows the mass fraction of fuel, radical and product profiles in the reaction zone behind the shock front. For a low value of $T_B = 0.85T_{shock}$, the chain-branching induction zone length is small and a significant buildup of chain radical concentration occurs rapidly. Since the chain-branching cross-over temperature $T_B$ is the temperature at which the chain-branching rate is equal to that of the chain termination, we see that for a low value of $T_B$, the chain-branching reaction rate is significantly greater than that of the recombination reaction and a relatively longer recombination region is obtained before the final equilibrium is reached. However, for higher values of $T_B$, the chain-branching induction zone increases, resulting in

a lower peak concentration of chain radicals. For high values of $T_B$, the rate of chain-branching reaction is lower, thus allowing the chain-termination reaction to become effective before all the reactants have been broken up into chain radicals. Hence, this restricts the buildup in free radical concentration in the reaction zone.

From the steady ZND analysis, we can see that the present three-step model allows us to vary the ratio between the induction zone length and reaction zone length independently (as described previously by Short & Quirk 1997). This is one of the distinct advantages over the standard one-step Arrhenius rate model. In fact, it is difficult to define an induction zone length in the one-step Arrhenius rate model where both induction and reaction length are governed only by a global activation energy.

### 3.2. *Unsteady detonation structure*

It is well known that a steady ZND solution may be unstable and the response of the steady-state solution to small perturbations can be obtained via a linear stability analysis such as those carried out by Erpenbeck (1964), Lee & Stewart (1990), Bourlioux *et al.* (1991), Sharpe (1997) or Short & Dold (1996), for example. Alternatively, the stability of a steady-state solution can be studied through an unsteady calculation from initial conditions, where the transient behaviour of the detonation is considered. Unsteady numerical simulations of one-dimensional detonations subject to the present three-step chemical kinetic model have already been performed by Short & Quirk (1997) to study the nonlinear stability of the structure of overdriven detonation waves. However, they have only considered the specific problem of overdriven detonations with overdrive factor $f = 1.2$. The stability analyses of idealized unsupported CJ detonations, to the best of the authors' knowledge, have not been performed previously with this three-step chemical kinetic model. In addition, Short & Quirk (1997) first assumed a steady ZND structure, and then subjected this stable solution to a perturbation. However, it has also not been established that the steady ZND profile of an unsupported CJ detonation with the present three-step chemical kinetic model can in fact be reached from an initial transient development. Hence, it is important to examine if the steady CJ detonation using the present three-step chemical kinetic description can indeed be formed from arbitrary initial conditions and also to describe its instability with the chosen combustible mixture parameters before actually focusing on the problem of direct initiation of detonation. An unsteady analysis of the transient development of a one-dimensional detonation initiated by a strong blast wave is thus carried out to determine the existence of the steady CJ detonation wave and its instability subject to the present three-step chemical kinetic model. Details of the initial conditions will be given later on when we discuss the direct initiation phenomenon.

The unsteady one-dimensional reactive Euler equations with the present chemical kinetic scheme are solved numerically using a detonation code based on the piecewise parabolic method (PPM) of Colella & Woodward (1984), which is a higher-order extension of a Godunov-type method, together with a conservative shock-front tracking algorithm (Chern & Collela 1987). Due to the small length scale of the present problem, it is important to properly refine the reaction zone. Therefore, an adaptive mesh refinement is used within the reaction zone (Berger & Collela 1989). This combination of numerical methods follows Bourlioux's (1991) approach. The computation domain is initially covered by a uniform coarse grid of 20 numerical cells per half-reaction zone length. An extra fine grid, with a refinement ratio of 5, giving an effective resolution of 100 cells per steady ZND half-reaction zone length (i.e. where

| Cross-over temperature $T_B$ | Ratio $\delta$ |
|---|---|
| $0.86T_{shock}$ | 0.891 |
| $0.90T_{shock}$ | 1.123 |
| $0.92T_{shock}$ | 1.240 |
| $0.93T_{shock}$ | 1.328 |
| $0.945T_{shock}$ | 1.429 |
| $0.95T_{shock}$ | 1.468 |

TABLE 1. The ratio $\delta$ for different chain-branching cross-over temperature $T_B$ obtained with $Q = 8.33$ and $\gamma = 1.2$, $E_I = 37.5$, $E_B = 10$ and $T_I = 3T_{shock}$.

half the chemical energy of the reaction has been released) is used within the reaction zone of the detonation. This high resolution ensures that each reaction step is well resolved (more than 20 cells were present within the zone of each reaction step). All computations are performed with a CFL number of 0.5. Validation and further details on the numerical methods used here can be found in the paper by Bourlioux *et al.* (1991). The present numerical code itself was initially developed by Mazaheri (1997) and extended to a three-step reaction mechanism for the present study.

In previous studies using a single-step Arrhenius rate law, the stability of the detonation wave is usually characterized by the global activation energy of the rate law. As the activation energy increases beyond the value for the stability limit, the detonation front changes from small harmonic oscillations to nonlinear pulsations and eventually to highly irregular behaviour when the activation energy is far from the stability limit value (He & Lee 1995). Similar phenomena are also observed when the degree of overdrive is reduced for a given unstable value of activation energy (Bourlioux *et al.* 1991). The activation energy is a parameter in the single-step rate law that can control the ratio between the induction- and reaction-zone lengths, i.e.

$$\delta = \frac{\Delta_{Induction}}{\Delta_{Reaction}}. \tag{3.3}$$

To understand more clearly the nonlinear pulsating instability of the detonation, we should emphasize the importance of the ratio $\delta$. To obtain it, the values of the induction-zone and reaction-zone length are defined from the heat-release curve as shown in figure 3. The black dot corresponds to the maximum of the heat release rate or the inflection point of the curve (see Borisov, Zamanskii & Lisyanskii 1987). The induction-zone length represents the extent of the thermally neutral portion in the total length of chemical reaction and the reaction-zone length approximately estimates the distance for the major part of the reaction heat to be released, or equivalently the explosion time.

For the three-step chemical kinetic model, the ratio between the induction-zone and reaction-zone lengths can be changed by varying the chain-branching cross-over temperature $T_B$, as discussed in § 3.1. Table 1 shows the corresponding value of the ratio $\delta$ for different chain-branching cross-over temperatures $T_B$.

### 3.2.1. *Stable detonation with* $\delta < 1$

Figure 4 shows the leading shock pressure versus the distance travelled by the shock front with the value of the chain-branching cross-over temperature $T_B$ equal to $0.86T_{shock}$ in the three-step chemical kinetic model. From the steady ZND structure, we know that for $T_B = 0.86T_{shock}$, the induction-zone length is short compared to the

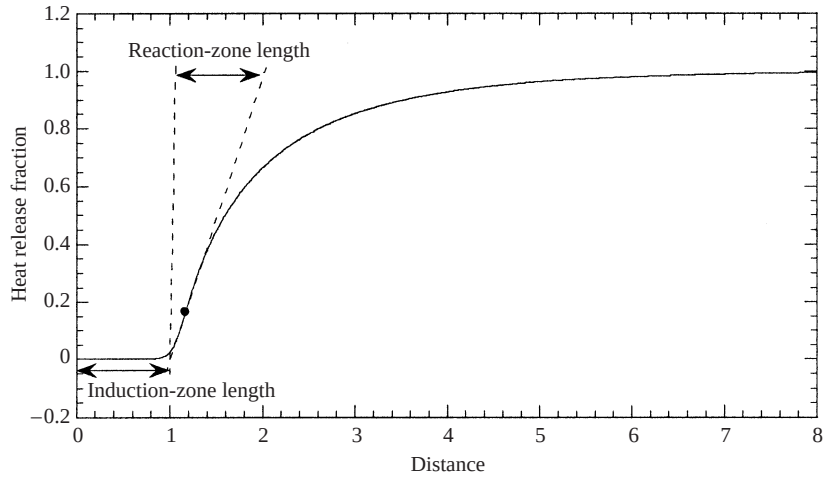


FIGURE 3. Heat release profile obtained with $Q = 8.33$, $\gamma = 1.2$, $E_I = 37.5$, $E_B = 10$, $T_I = 3T_{shock}$ and $T_B = 0.90T_{shock}$ for the three-step chemical kinetic model.

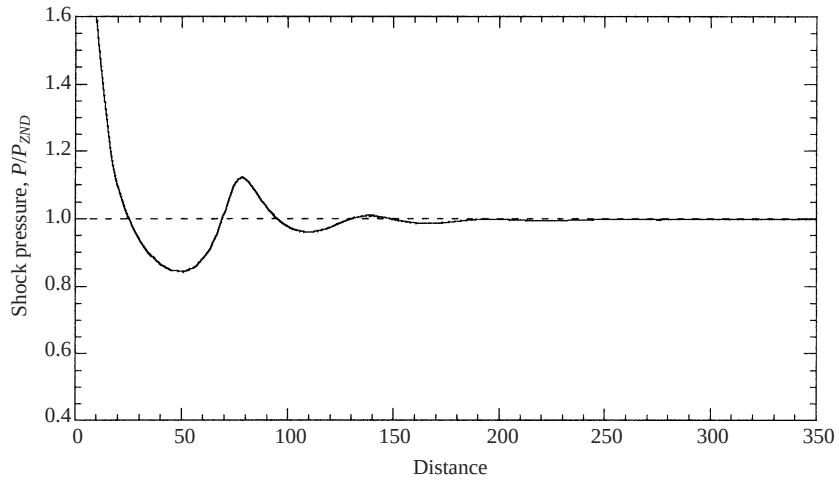


FIGURE 4. Leading shock pressure versus position for a stable detonation wave with $T_B = 0.86T_{shock}$ for the three-step chemical kinetic model.

recombination- or reaction-zone length. In this case, the ratio $\delta$ is found to be 0.891. At early time, a small-amplitude oscillation is observed due to the unsteady initiation process. However, after a period of time, the oscillation is damped out and the detonation wave eventually approaches to a stable steady-state solution. Comparison between the detonation profiles obtained from the steady ZND calculation and a transient calculation is shown in figure 5($a, b$), showing good agreement. Here, we can see that for small ratio $\delta$ (less than 1), the steady detonation wave is stable to a small perturbation and a steady ZND solution can be achieved from arbitrary initial conditions after the long-time evolution.

### 3.2.2. *Unstable detonation with* $\delta \approx 1$

By increasing the chain-branching cross-over temperature $T_B$ to $0.92T_{shock}$, thereby increasing the chain-branching induction length relative to the length of the recom-

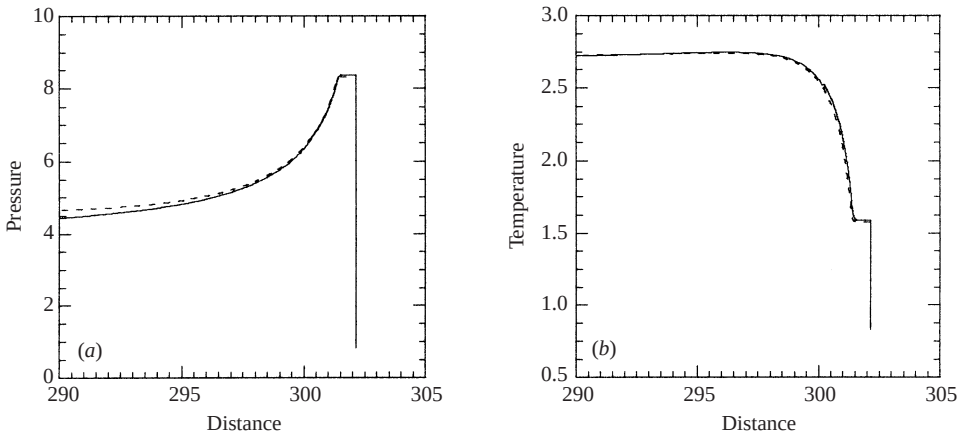


FIGURE 5. Comparison between the steady ZND solution (dashed lines) and the long-time solution from transient calculation (solid lines) with $T_B = 0.86T_{shock}$ for the three-step chemical kinetic model. (*a*) Pressure profile; (*b*) temperature profile.

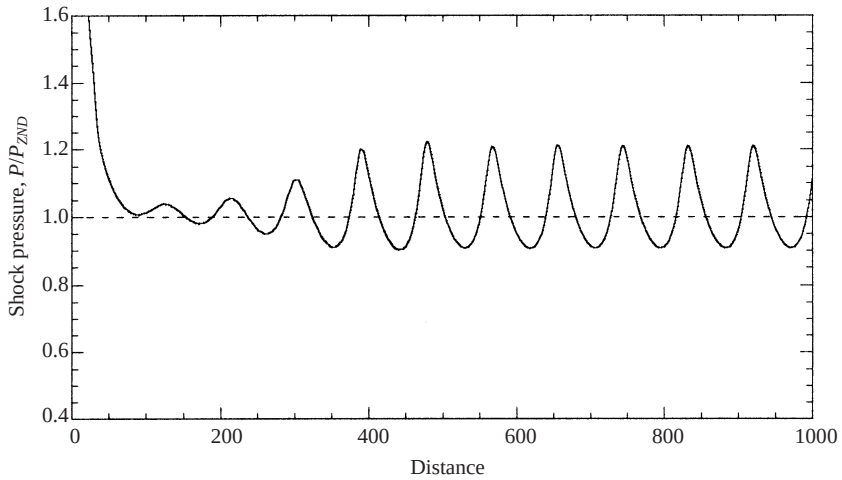


FIGURE 6. Leading shock pressure versus position for an unstable detonation wave (a single-mode oscillation) with $T_B = 0.92T_{shock}$ for the three-step chemical kinetic model.

bination region and giving a value of $\delta$ greater than 1, an unstable detonation wave is obtained from the blast wave decay, as shown in figure 6. Hence for high values of $T_B$, a stable detonation cannot be achieved from a transient calculation. For $T_B = 0.92T_{shock}$, the oscillation demonstrates a regular oscillatory behaviour with constant period. This phenomenon is generally referred to as a pulsating detonation and it is found in the present computation that this instability starts to occur when the ratio $\delta$ is close to unity (with $T_B \sim 0.90T_{shock}$). A longer induction-zone length compared to the reaction length therefore renders the system unstable. The instability mechanism underlying the steady constant-period pulsation is thought to be due to the periodic low-frequency, finite-amplitude compression and expansion waves in the chain-branching induction zone between the main reaction region of the reaction zone and the leading shock (Short *et al.* 1999).

Further increase in the chain-branching cross-over temperature $T_B$ for the three-step kinetic model causes the oscillation to become less regular. The ratio $\delta$ eventually

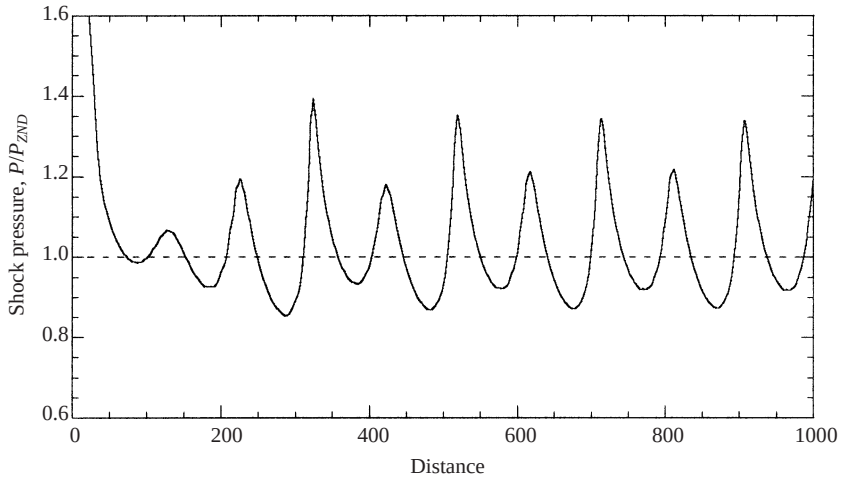


FIGURE 7. Leading shock pressure versus position for an unstable detonation wave (a period-doubling bifurcation) with $T_B = 0.93T_{shock}$ for the three-step chemical kinetic model.

becomes much larger than 1. For $T_B = 0.93T_{shock}$, a bifurcation occurs. The instability of the detonation front migrates from a regular single-mode oscillation to a steady period-doubled oscillation after some transient development, as illustrated in figure 7. It consists of a high-amplitude oscillation followed by a smaller-amplitude oscillation.

### 3.2.3. *Highly unstable detonation with* $\delta > 1$

For a very large value of $T_B$, a very long chain-branching induction zone occurs which can significantly affect the propagation of detonation waves. A highly non-steady behaviour with a number of oscillations of different amplitudes and periods is observed, as shown in figure 8. The shock pressure fluctuation varies between 0.7 and $2.0P_{ZND}$. This result shows that no steady solution can be obtained. The oscillation is irregular and is often called a multi-mode pulsating detonation. In this case, the instability mechanism is more complex because a secondary detonation is formed behind the leading detonation shock and thus results to a shock–shock interaction. This accounts for the observation of the highly irregular behaviour.

### 3.2.4. *Detonability limit for* $\delta \gg 1$

If the chain-branching cross-over temperature $T_B$ continues to increase further, then at some critical value of $T_B$ (i.e. $T_B = 0.95T_{shock}$ giving a ratio $\delta = 1.468$), the detonation wave fails. This phenomenon is shown in figure 9. For sufficiently large $T_B$, the reaction zone (where the chemical energy is released) is at a distance far away from the shock front. With a large-amplitude fluctuation, the shock temperature will drop below the chain-branching cross-over temperature $T_B$. The rate constant for the chain-branching reaction then becomes very small and has a profound effect on the rate of radical production behind the shock. The chain-branching reaction is eventually 'switched off' and overridden by the chain-termination reaction. Therefore, decoupling between the detonation shock and reaction zone occurs. The energy released from the reaction zone cannot sustain the detonation wave and, hence, the detonation wave quenches.

From the numerical results using a single-step chemical kinetic model, He & Lee (1995) found that the dynamic quenching phenomenon due to instability occurs only

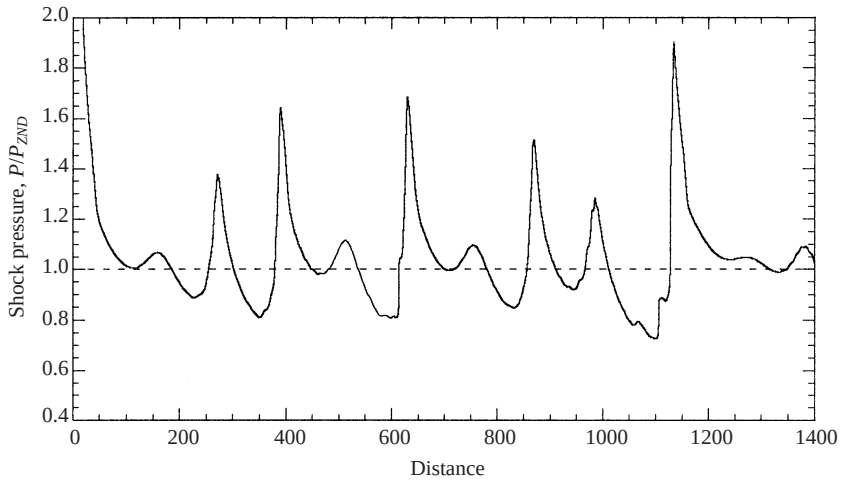


FIGURE 8. Leading shock pressure versus position for an unstable detonation wave (a multi-mode oscillation) with $T_B = 0.945T_{shock}$ for the three-step chemical kinetic model.

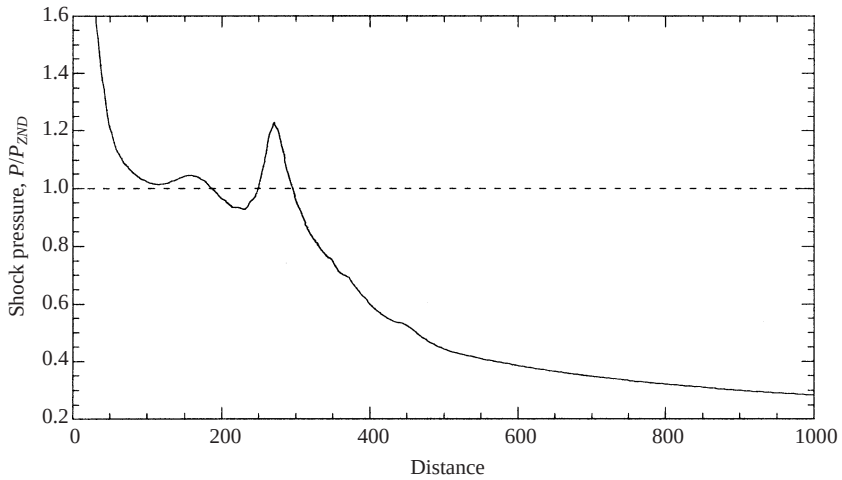


FIGURE 9. Quenching of detonation wave: detonability limit with $T_B = 0.95T_{shock}$ for the three-step chemical kinetic model.

at a very high value of activation energy. They mentioned that there exists a dynamic limit of activation energy for which the detonation cannot propagate via the auto-ignition mechanism. However, Sharpe & Falle (1999) recently found that even at a high value of activation energy for the one-step Arrhenius rate law, the detonation wave still propagates as a series of explosions if one uses a very refined numerical grid for the computation. Therefore, for single-step chemistry, there is no clear definition for this detonation limit. Unlike a detonation wave using a one-step Arrhenius chemical reaction, a clearer criterion for the failure can now be established using the present three-step kinetic model. From a purely chemical kinetic consideration, Short & Quirk (1997) in their paper state that: 'If the detonation shock temperature drops to the chain-branching cross-over temperature $T_B$, the detonability limit occurs'.

This criterion is significant and will be applied later to the problem of direct initiation of detonation. Similar to Short & Quirk's (1997) results, the present simulations

also demonstrate that the pulsating behaviour found for the three-step reaction model is similar to the pulsating detonation instabilities found for the standard one-step reaction model observed in previous investigations (Fickett & Wood 1966; He & Lee 1995, for example). However, the chemical switch-off mechanism in this multi-step reaction model that causes the quenching to occur is not present for one-step Arrhenius reaction kinetics.

It is suggested that the ratio between the induction-zone and reaction-zone lengths is the main parameter (independent of the rate process) which characterizes the stability of detonation waves. The significance of these two length scales for the detonation stability has been discussed by Short & Quirk (1997) and also experimentally observed by Borisov *et al.* (1987). In the present study, we also observe qualitatively that if the value $\delta$ is much smaller than 1, where the reaction-zone length is always larger than the induction-zone length, the detonation wave is stable. When the value $\delta$ approaches one, the detonation starts to become weakly unstable. This implies that as soon as the induction stage of the reaction becomes dominant, the wave is unstable to perturbations and a regular oscillation of the detonation front can be observed. If this ratio is much larger than 1, the shock front oscillates in a highly irregular manner with different amplitudes and eventually the detonation limit occurs due to the large fluctuation of the detonation front.

Since this ratio offers a reasonable explanation of some important features of detonations, in the following section this ratio will be used to characterize the mixture, for simplicity.

## 4. Direct initiation of detonation

After having examined the detonation structure and its associated instability in the previous section, the phenomenon of direct initiation of detonation is now investigated for planar, cylindrical and spherical geometries with the three-step chemical kinetic model. We shall adopt the ideal strong blast wave model as initial conditions, the same approach as in most of the previous studies (Mazaheri 1997; Eckett *et al.* 2000). For ideal strong blast waves, the initial conditions are given by the similarity solution of Taylor (1950) and Sedov (1959). The subsequent decay of the blast, when chemical reaction comes into play, must be described by the numerical integration of the reactive Euler equations with the appropriate chemical rate law. For a perfect gas with constant specific heat ratio $\gamma$, the similarity solution of the point blast model consistent with earlier normalization is given by

$$\left.\begin{aligned} &u_s = \frac{2}{\gamma+1}M_s, \quad p_s = \frac{2}{\gamma+1}M_s^2, \quad \rho_s = \frac{\gamma+1}{\gamma-1}, \\ &\frac{u}{u_s} = f\left(\frac{r}{R_s}\right), \quad \frac{\rho}{\rho_s} = g\left(\frac{r}{R_s}\right), \quad \frac{p}{p_s} = h\left(\frac{r}{R_s}\right), \end{aligned}\right\} \tag{4.1}$$

where subscript $s$ refers to the conditions immediately after the shock. $M_s$ and $R_s$ denote the shock Mach number and shock radius respectively. The spatial distribution of flow variables behind the blast wave, i.e. velocity $u$, density $\rho$ and pressure $p$, can be obtained by solving the functions $f(r/R_s)$, $g(r/R_s)$ and $h(r/R_s)$, which are listed in the book by Korobeinikov (1991). Likewise, the similarity solution for non-reacting strong blast waves also gives the following relationship between the strength of the shock $M_s$, the shock radius $R_s$ and the non-dimensional source energy $E_s$, respectively

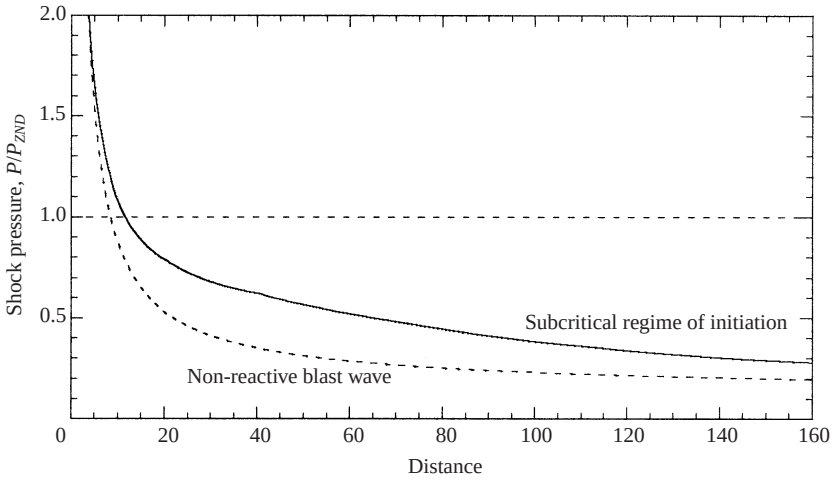


FIGURE 10. Leading shock pressure versus position for the subcritical regime of planar initiation obtained with $Q = 8.33$, $\gamma = 1.2$, $\delta = 0.604$ and non-dimensional initiation energy $E_s = 350$. (The dashed lines represent the non-reactive blast wave.)

per unit area, per unit length, or just the energy itself for the three geometries:

$$E_s = \frac{\tilde{E}_s}{\tilde{p}_o \tilde{r}_c^{j+1}} = \alpha_j \left(\frac{j+3}{2}\right)^2 \gamma M_s^2 R_s^{j+1}, \tag{4.2}$$

where $\alpha_j$ is the energy integral constant ($\alpha_1 = 2.257$, $\alpha_2 = 2.026$, $\alpha_3 = 1.739$ obtained from the correlations given by Korobeinikov 1991), which is a function of the adiabatic exponent $\gamma$. Also, $\tilde{p}_o$ is the dimensional initial pressure of the mixture and $j$ is the geometric index, i.e. $j = 0$, 1, 2 for the planar, cylindrical and spherical geometries, respectively. Knowing the initial shock strength and location, the initiation source energy can be determined from this relationship.

### 4.1. *The three regimes of direct initiation*

From the experimental investigation of direct initiation of spherical detonation by Bach, Knystautus & Lee (1969), we know that the initiation process can be classified into three regimes, i.e. subcritical, supercritical and critical, according to whether the ignition source energy is less than, greater than, or equal to a threshold value corresponding to the critical energy. The three regimes of direct initiation are first simulated for planar geometry and their mechanism is discussed in this section. A mixture that corresponds to a hydro-dynamically stable detonation (with $\delta$ less than 1) is first investigated.

#### 4.1.1. *The subcritical regime*

Upon the sudden deposition of a large amount of energy in a gaseous combustible mixture, a strong blast wave is formed. During the early times of the blast wave propagation, the shock pressure decreases rapidly as for a strong non-reactive blast wave since the blast energy dominates the decay process. As the blast decays to larger distances, the chemical heat release starts to influence the blast wave propagation (at about $M_s < 1.5 M_{CJ}$). If the source energy is far below the critical value, the chemical reaction zone fails to couple to the shock front and the blast continues to decay to the sonic speed. This initiation phenomenon is referred to the subcritical regime of initiation where the source energy is below the critical value. Figure 10 shows

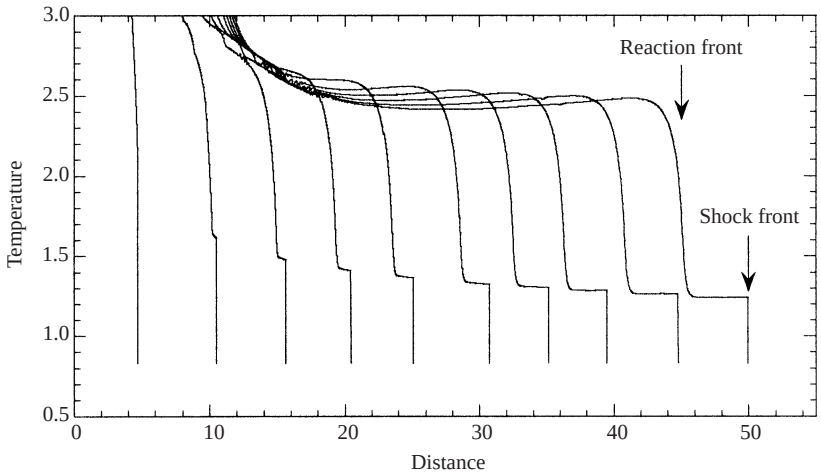


FIGURE 11. Temperature profiles at different times for the subcritical regime of planar initiation obtained with $Q = 8.33$, $\gamma = 1.2$, $\delta = 0.604$ and non-dimensional initiation energy $E_s = 350$.

the leading shock pressure versus position for the subcritical regime of initiation, together with that of a non-reactive blast wave for comparison. In this case, the non-dimensional planar initiation energy $E_s$ is equal to 350. As the blast wave continues to decay, the combustion front will recede further from the shock front. The shock progressively decays to sonic velocities, similar to non-reactive blast wave propagation, while the combustion zone propagates as a slow deflagration wave.

The decoupling between the reaction front and the leading shock can be clearly observed from the temperature profiles. Figure 11 shows the temperature profiles at different times during the blast decay. In the subcritical regime, two sharp temperature rises can be seen in the profiles. The first abrupt rise in the temperature is due to the shock compression. A short plateau follows where the temperature remains almost constant. This distance corresponds to the induction zone length, i.e. the region where the 'incubation' process takes place and the reactants start to dissociate into free radicals. After the induction period, the chemical energy release starts because the recombination process of radicals is exothermic. Thus, a second rise in temperature occurs due to the rapid chemical heat release. This second jump in temperature is defined as the reaction front. In the early times of blast wave propagation, the induction zone is extremely short (almost not perceptible) due to the high temperatures. Thus, the two fronts are coupled and cannot be distinguished from each other. However, as the blast decays to weaker strength, the shock temperature is lower and the induction time increases. The shock and the reaction fronts start to decouple as the induction length increases.

The reason for the decoupling phenomenon can be explained by looking at the profiles of the mass fraction of fuel and radical (see figure 12). Early in the decay of the blast, the chain-branching induction zone is small and there is still a significant buildup of chain radical concentration at the combustion front. As the blast expands further, the rate of the chain-branching reaction decreases, resulting in a lower peak concentration of the chain radicals. Once the temperature drops below the chain-branching cross-over temperature $T_B$, the chain-branching reaction step is essentially 'switched off' and eventually no further radical buildup can be observed in the reaction zone. This leads to a significant increase in the induction-zone length and results in a complete decoupling of the combustion front and the leading shock.

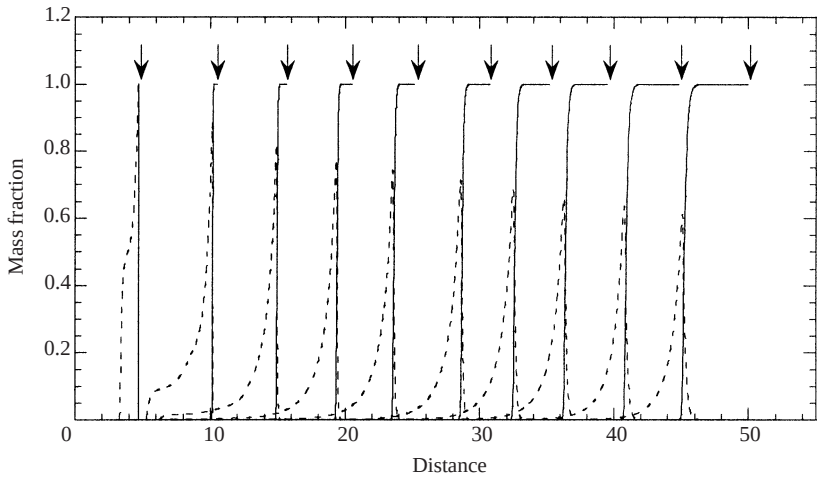


FIGURE 12. Detonation structure profiles showing the mass fraction of fuel (solid lines) and radical (dashed lines) for the subcritical regime of planar initiation obtained with $Q = 8.33$, $\gamma = 1.2$, $\delta = 0.604$ and non-dimensional initiation energy $E_s = 350$. The arrows indicate the leading shock front.

4.1.2. *The supercritical regime*

If the blast wave generated by the source is of sufficient duration, rapid auto-ignition takes place behind the blast wave and the chemical reaction zone is then intimately coupled with the shock. The blast wave decays continuously toward a self-sustained CJ detonation. The detonation front will continue to propagate steadily at the CJ velocity thereafter. This corresponds to the so-called supercritical regime of initiation. For the supercritical case, the amount of initiation energy is much larger than the critical value and the flow field simply consists of a blast wave continuously decaying to the CJ velocity of the mixture. The supercritical regime is illustrated in figure 13 which shows the shock front pressure in terms of the distance travelled by the shock for the supercritical regime of initiation. This simulation is performed with a non-dimensional planar initiation energy $E_s = 658$.

Figure 14 shows the temperature profiles for the supercritical regime of initiation. From this figure, we note that the temperature rise due to the heat release by combustion almost coincides with the temperature rise due to shock front compression. This indicates that the combustion front is intimately coupled to the shock front throughout. From the mass fraction of fuel and radical profiles (see figure 15), we also note that there is always a significant amount of chain radicals in the reaction front.

4.1.3. *The critical regime*

If the initiation energy is near the critical value, the phenomenon is more complex as illustrated in figure 16. Here, the non-dimensional source energy for the planar initiation has a value of 362. When the initiation energy is near the critical value, the shock front and the reaction front first decouple as the blast expands. The reaction front recedes from the leading shock. However, unlike the subcritical case, where the reaction zone continually recedes from the shock, the decoupling in the critical case stops after the blast wave has decayed to a certain shock velocity. Thereafter both the shock and the reaction front propagate together as a quasi-steady complex at a Mach number near the auto-ignition limit of the mixture. This is referred to

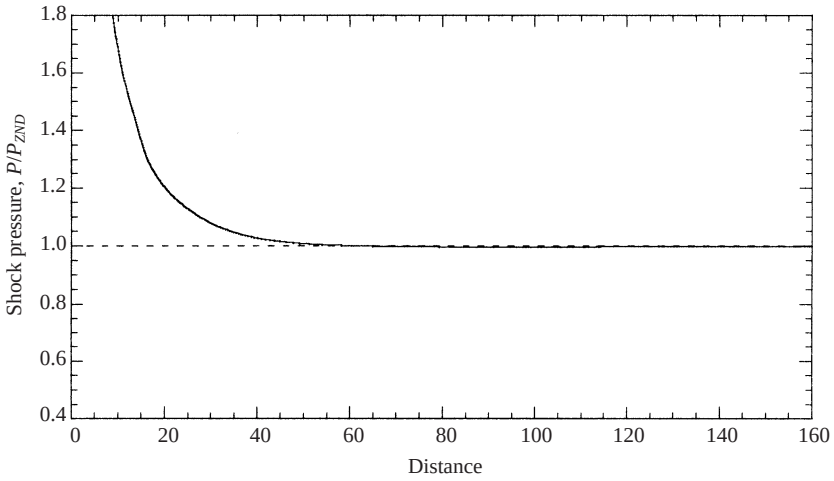


FIGURE 13. Leading shock pressure versus position for the supercritical regime of planar initiation obtained with $Q = 8.33$, $\gamma = 1.2$, $\delta = 0.604$ and non-dimensional initiation energy $E_s = 658$.

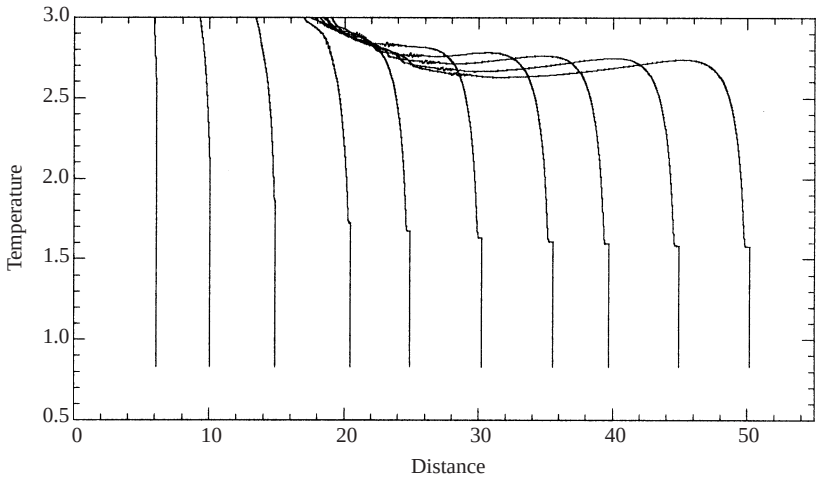


FIGURE 14. Temperature profiles at different times for the supercritical regime of planar initiation obtained with $Q = 8.33$, $\gamma = 1.2$, $\delta = 0.604$ and non-dimensional initiation energy $E_s = 658$.

as the quasi-steady period and this quasi-steady period terminates when the shock front abruptly re-accelerates to form an overdriven detonation wave. The overdriven wave eventually decays to a self-sustained detonation wave. If the initiation energy is smaller than this critical value, the decoupling will continue and the shock will eventually decay to an acoustic wave ($M_s = 1$) and no detonation is initiated, as in the subcritical case.

Figure 17 shows the temperature profiles at different times for the critical regime of initiation. During the early blast decay, the distance between the reaction and shock fronts progressively increases as they decouple from each other. Near the end of the quasi-steady period, the distance between these two fronts decreases again and the shock begins to accelerate and finally the two fronts become completely coupled. The shock temperature corresponds closely to the chain-branching cross-over temperature $T_B$ in the quasi-steady regime. The same phenomena can be observed in figure 18 showing the mass fraction of reactant and radical during the initiation process.

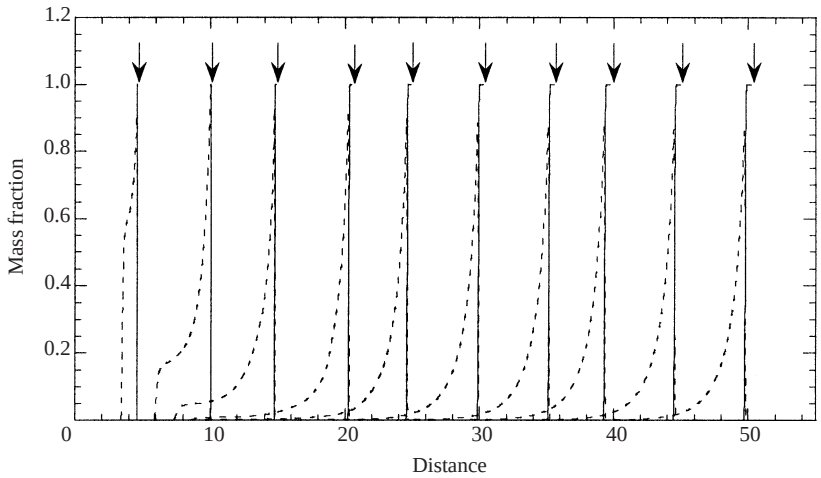


FIGURE 15. Detonation structure profiles showing the mass fraction of fuel (solid lines) and radical (dashed lines) for the supercritical regime of initiation obtained with $Q = 8.33$, $\gamma = 1.2$, $\delta = 0.604$ and non-dimensional initiation energy $E_s = 658$. The arrows indicate the leading shock front.

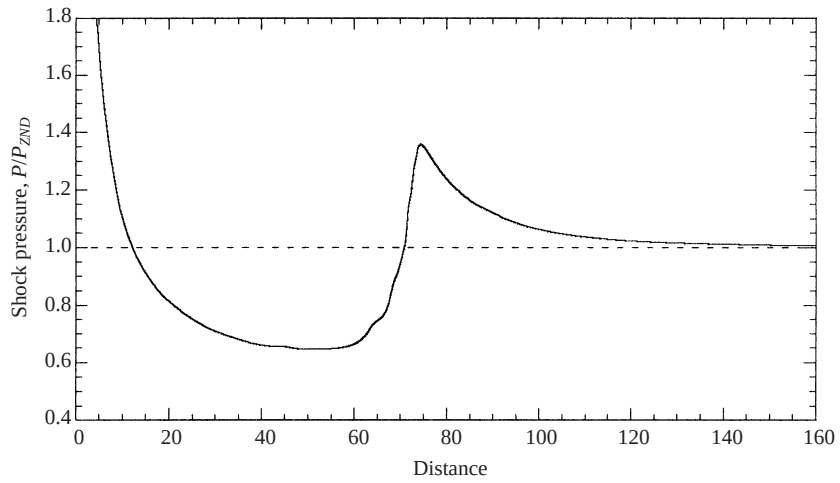


FIGURE 16. Leading shock pressure versus position for the critical regime of planar initiation obtained with $Q = 8.33$, $\gamma = 1.2$, $\delta = 0.604$ and non-dimensional initiation energy $E_s = 362$.

To understand the re-acceleration process before the onset of detonation, some observations can be made from the analysis of the pressure profiles. Figure 19 shows the pressure profiles for the critical regime of initiation. Early in the decay, the shock pressure and the pressure gradient at the shock are decreasing as the shock moves forward. A pressure pulse begins to develop in the region between the reaction front and the leading shock. As the reaction–shock complex moves, this pressure pulse starts to amplify. This pressure pulse eventually becomes the maximum pressure in the flow field. The distance between the reaction front and the peak pressure decreases as the structure moves. As the strength of the pressure pulse increases, the shock front accelerates because the high-pressure region begins to drive the shock front. The leading shock and the reaction front eventually merge together to form an overdriven detonation and subsequently relax to the CJ detonation. This initiation process

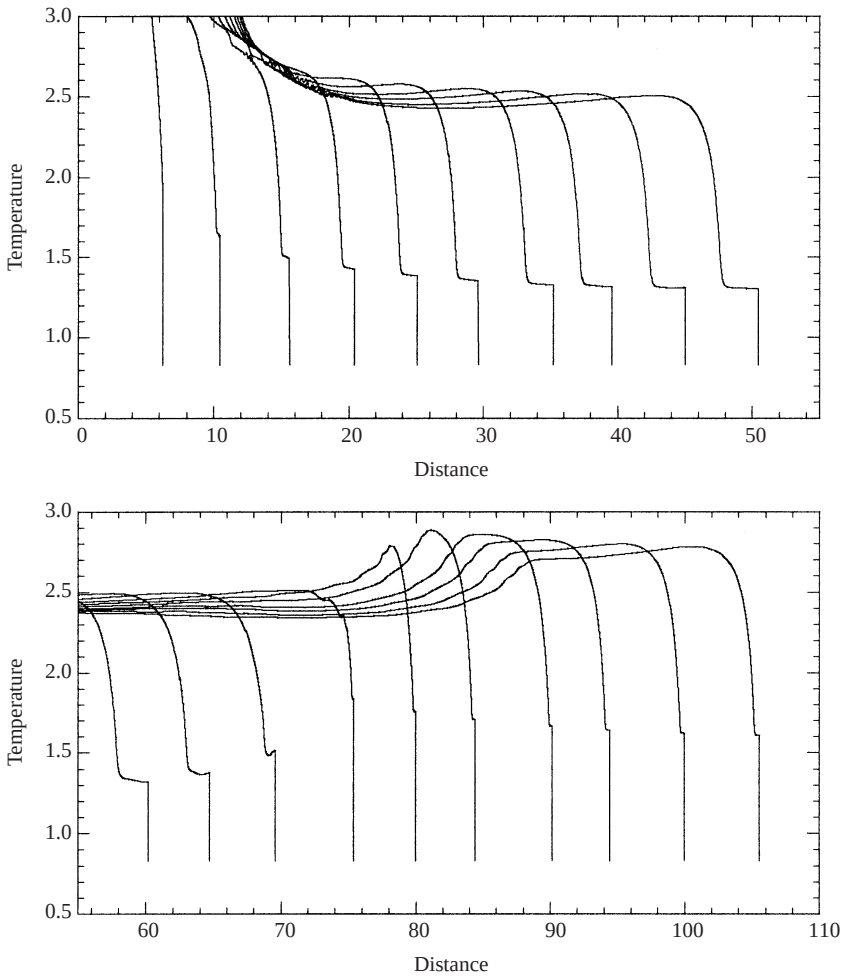


FIGURE 17. Temperature profiles at different times for the critical regime of planar initiation obtained with $Q = 8.33$, $\gamma = 1.2$, $\delta = 0.604$ and non-dimensional initiation energy $E_s = 362$.

has also been observed in previous numerical simulations of detonation initiation (Mazaheri 1997; Eckett *et al.* 2000). Although not addressing direct blast initiation per se, a similar feature is also noticed by Clarke and co-workers (Clarke, Kassoy & Riley 1986; Clarke *et al.* 1990) in their investigation of the detonation initiation problem using other means of initiation, i.e. by a heated layer of gas and piston-driven shock. The mutual interaction of the pressure pulse and the chemical heat release results in the rapid amplification of the pressure pulse and the onset of a detonation. This is the essence of the mechanism of shock wave amplification by coherent energy release (SWACER), proposed by Lee (see Lee & Moen 1980). This process of rapid shock amplification at the end of the quasi-steady period can be explained by the fact that the chemical energy release in the reaction front is synchronized with the propagation of the pressure pulse within the reaction–shock complex.

The results from simulations clearly demonstrate that it is the re-acceleration of the wave after an initial decoupling of the reaction front from the blast which is responsible for the initiation in the critical regime. Therefore, all existing initiation

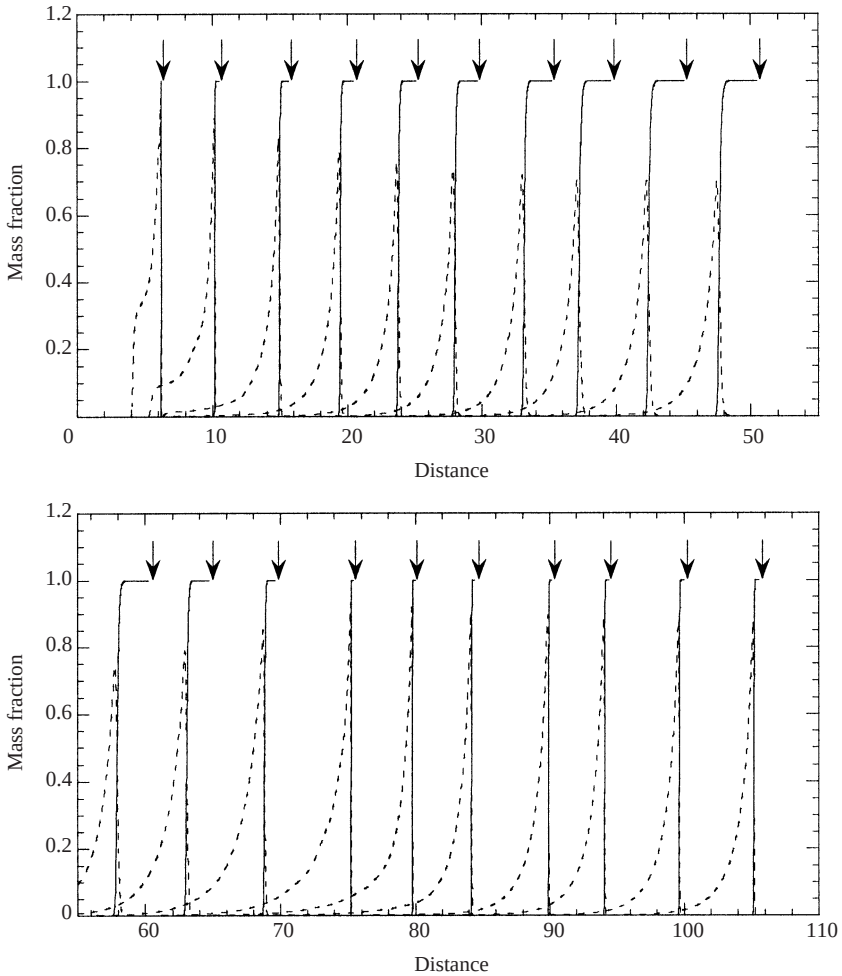


FIGURE 18. Detonation structure profiles showing the mass fraction of fuel (solid lines) and radical (dashed lines) for the critical regime of planar initiation obtained with $Q = 8.33$, $\gamma = 1.2$, $\delta = 0.604$ and non-dimensional initiation energy $E_s = 362$. The arrows indicate the leading shock front.

theories based on a failure criterion due to curvature (He & Clavin 1994) or quenching due to unsteadiness (Eckett *et al.* 2000) of the decaying blast wave may not be sufficient to fully describe the direct initiation phenomenon. These initiation theories only consider the first phase of the initiation process where a critical condition is being prepared from the blast wave decay for the second phase of rapid shock amplification. These models can be adequate for predictive purposes, but lack the ability to describe the complete initiation process. Therefore, a better criterion should take into account the mechanism of the amplification process at the end of quasi-steady period. Effective shock wave amplification depends on whether or not a reacting flow-field maintains the SWACER mechanism for a sufficiently long duration and the chemistry should play a significant role in this process. Hence, it is important to use a multi-step chemical kinetic model to study the direct initiation since various parameters, such as the induction time gradient, reactivity of gas mixture, etc, should govern the SWACER mechanism.

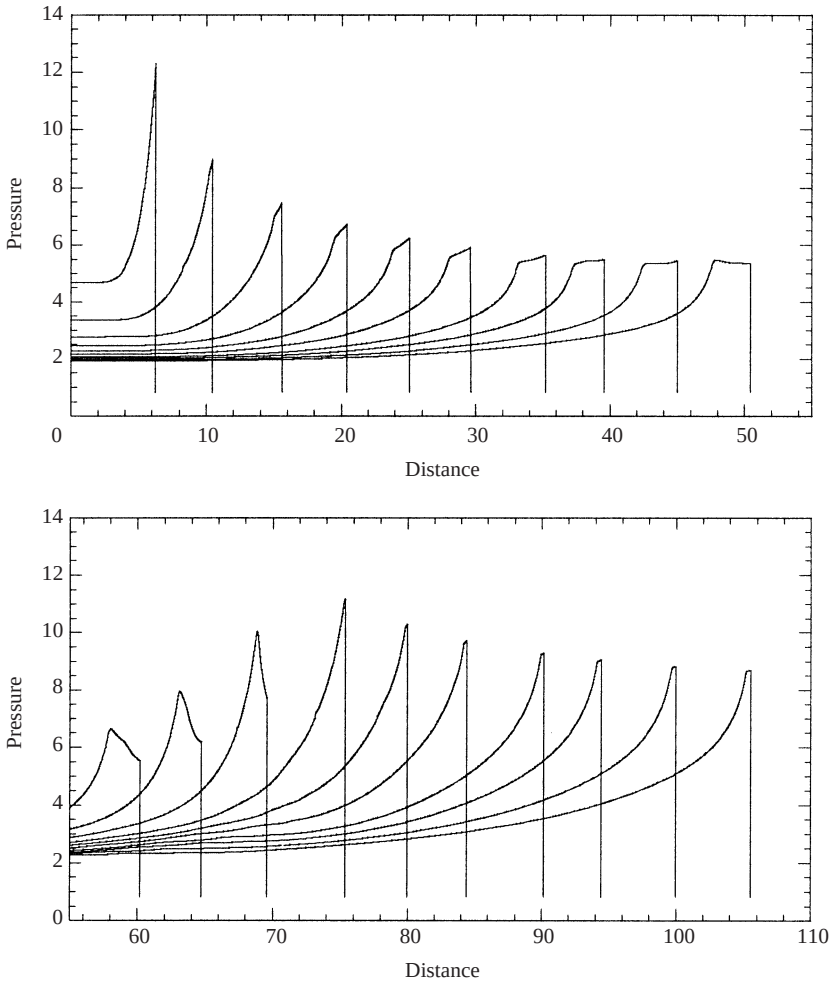


FIGURE 19. Pressure profiles at different times for the critical regime of planar initiation obtained with $Q = 8.33$, $\gamma = 1.2$, $\delta = 0.604$ and non-dimensional initiation energy $E_s = 362$.

### 4.2. *The effect of instability on the initiation*

The initiation process for stable detonation was studied in the previous section. Similar calculations are presented here for unstable mixtures (with $\delta$ greater than 1). As mentioned in § 3.1, if the induction length is increased relative to the recombination-zone length, the detonation wave becomes unstable. We have introduced the ratio $\delta$ as the main parameter controlling the stability of one-dimensional pulsating detonations. An interesting question that arises is whether the instability of the detonation plays a role in the initiation process.

For comparison, figure 20 and figure 21 show the pressure of the shock front versus position for stable and highly unstable detonations of planar geometry, respectively. For the stable case with $\delta = 0.604$, the initiation process can be well described by the decay of the blast wave. The blast wave decays to a sub-CJ value and re-accelerates back to the CJ detonation after the quasi-steady period. Therefore, the critical initiation energy can be well approximated from the blast wave theory. The numerical result shows that some new phenomena appear for highly unstable

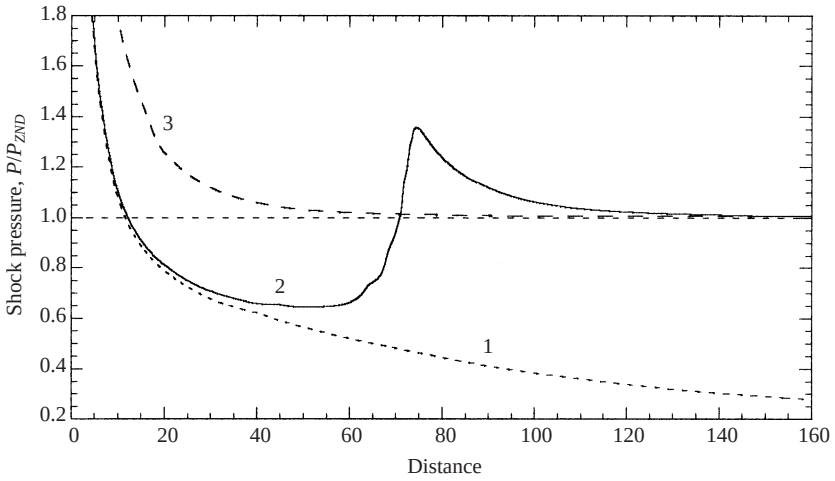


FIGURE 20. Leading shock pressure versus position for the direct initiation of a stable detonation obtained with $Q = 8.33$, $\gamma = 1.2$, $\delta = 0.604$ and different non-dimensional initiation energies: $E_{s_1} = 350$, $E_{s_2} = 362$ and $E_{s_3} = 746$.

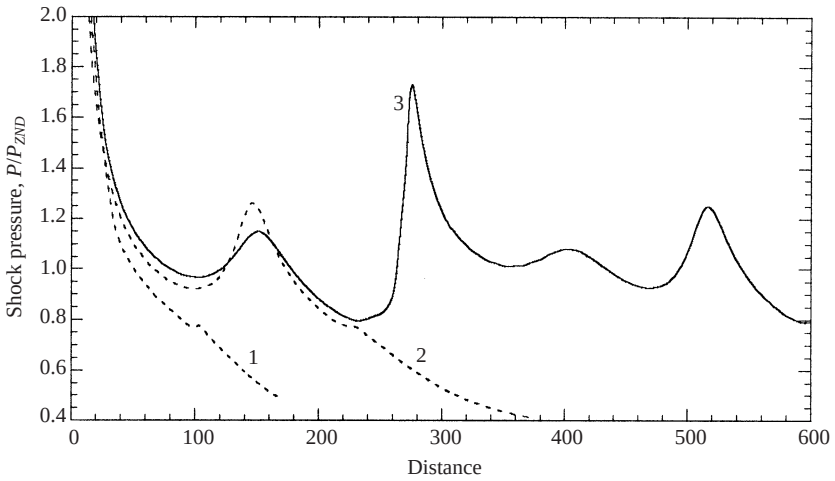


FIGURE 21. Leading shock pressure versus position for the direct initiation of a highly unstable planar detonation obtained with $Q = 8.33$, $\gamma = 1.2$, $\delta = 1.429$ and different non-dimensional initiation energies: $E_{s_1} = 1195$, $E_{s_2} = 1371$ and $E_{s_3} = 1445$.

detonation ($\delta = 1.429$), where the final self-sustained detonation propagates with an irregular behaviour. Instead of the blast decaying continuously to the sub-CJ value, oscillation occurs during the initiation process. The detonation instability clearly influences the initiation process. For curve 1, the source energy is far from the critical value. The reaction front and the shock are decoupled throughout. The blast wave continues to decay to an acoustic wave. Curve 2 demonstrates how instability of the detonation front may induce some failure of the detonation. After the first oscillation of the shock pressure, it is possible that some unsteady event from the rear boundary of the reaction zone dominates the wave propagation and causes the quenching of the detonation wave. Therefore, a larger amount of initiation energy is expected to overcome all these instability effects of the detonation. The mechanism behind this initiation process for highly unstable detonation is beyond the scope of this work.

From these results we can see that the detonation instability is also important for the initiation process. So far, this instability effect has not been explicitly considered in any of the current initiation models. These models are mostly based on the blast wave theory and do not include a stability parameter in their formulations.

### 4.3. *Other geometries*

What we have considered so far is the initiation for planar detonation. For the planar case, the detonation wave is not subject to any curvature effect and only unsteadiness of the flow behind the shock causes the decay of the wave. For cylindrical and spherical detonations, curvature will be a factor in addition to unsteadiness and we shall investigate these combined effects on the initiation process. Curvature of a shock front induces an additional expansion of the gas behind it, and this additional expansion causes cooling and can lead to quenching of the chemical reactions. When a fluid particle crosses a curved shock wave, it is first compressed by the shock and its temperature is increased. Subsequently, the compressed fluid particle expands volumetrically due to the radial, outward flow behind the shock and this expansion will then result in a decrease in the temperature. The expansion of the fluid particle can cause failure of the detonation if the decrease in temperature is sufficiently rapid to quench the chemical reactions. To illustrate the curvature effect, consider the critical tube diameter phenomenon. When a detonation emerges abruptly from a confined tube into an open space, the planar detonation diffracts into a curved front. The wave fails if the curvature is excessive. Hence the tube diameter must be above some critical value so that the wave curvature does not lead to failure.

In the initiation of cylindrical and spherical detonations, the curvature decreases as the blast expands. However during the initiation process, both curvature and unsteadiness can cause failure of the diverging wave. Figure 22($a, b$) shows the shock front pressure versus position for the three regimes of initiation for cylindrical and spherical geometries. Since curvature can cause additional quenching, initiation of cylindrical detonation requires that the same critical strength of blast occurs at a larger radius than the planar geometry. Similarly, spherical detonation has even larger curvature at the same radius. Hence, the same critical value of the strength of the blast must be maintained to even larger radius than the cylindrical geometry in order for successful initiation to be achieved.

The three regimes of initiation for stable detonation are qualitatively similar for all three geometries. The only difference is that for the planar geometry a self-sustained detonation is formed closer to the source. Another interesting result is that the detonation velocity is found to be slightly lower than the planar ZND solution. Since the curvature term is proportional to $j/r$ in the conservation equations ($j = 1, 2$ for cylindrical and spherical geometries, respectively), then the velocity is always unsteady and only reaches the CJ value if the radius approaches infinity.

Another interesting phenomenon for diverging detonation waves is that curvature enhances the instability. Figure 23 shows the numerical results of unstable cylindrical detonation with a ratio $\delta = 0.891$. Although this value of $\delta$ corresponds to a stable case for planar detonation (see § 3.2), in the case of cylindrical detonation, instability occurs when the radius of the front is small. For the curved detonation front, the particle undergoes an expansion behind the shock due to the curvature effect. This expansion due to curvature increases the induction time and hence enhances the instability of the detonation wave. This is even more significant for spherical detonation because of the higher curvature. In this case, the wave will only become stable at the long time limit when the radius approaches infinity.

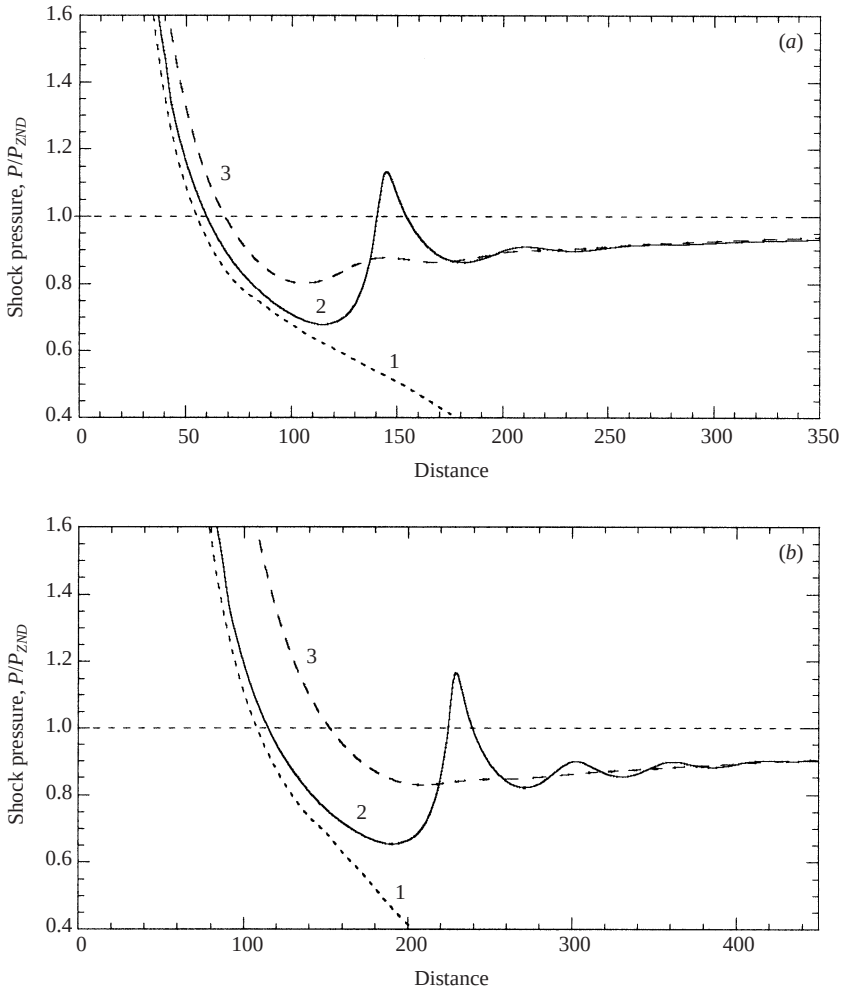


FIGURE 22. Three regimes of direct initiation obtained with $Q = 8.33$, $\gamma = 1.2$, $\delta = 0.604$. (*a*) Cylindrical geometry with non-dimensional initiation energies: $E_{s_1} = 1.08 \times 10^5$, $E_{s_2} = 1.14 \times 10^5$ and $E_{s_3} = 1.40 \times 10^5$; (*b*) spherical geometry with non-dimensional initiation energies: $E_{s_1} = 6.06 \times 10^7$, $E_{s_2} = 6.37 \times 10^7$ and $E_{s_3} = 1.56 \times 10^8$.

### 4.4. *The critical initiation energy*

Previous numerical studies on direct initiation of detonation using a single-step Arrhenius rate law failed to yield a clear value of the critical initiation energy (Mazaheri 1997). This contradicts experimental observations where a distinct value for the critical initiation energy is obtained. To illustrate the problem of using a single-step reaction rate law, the initiation processes of planar detonation for different initiation energies are plotted in figure 24. Note that if one waits long enough, then even curve 7 will eventually result in detonation initiation. Of course the time one has to wait increases exponentially, but no sharp cut-off can be obtained with a single-step model to permit an definitve value of the critical energy to be determined.

However if a more detailed chemical kinetic model is used, the difficulty in identifying the critical energy can be eliminated. A single-step rate model also does not provide a detonability limit. However, using a three-step reaction model, Short

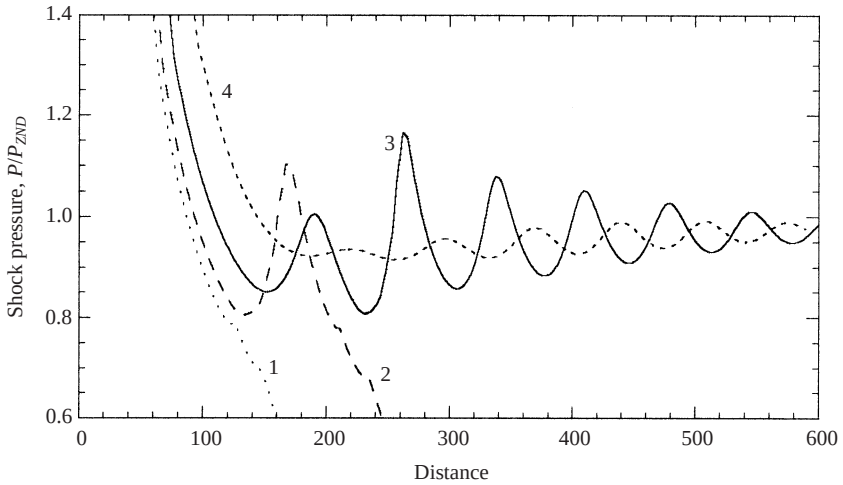


FIGURE 23. Direct initiation of unstable cylindrical detonation for $Q = 8.33$, $\gamma = 1.2$, $\delta = 0.891$ with non-dimensional initiation energies: $E_{s_1} = 2.74 \times 10^5$, $E_{s_2} = 3.01 \times 10^5$, $E_{s_3} = 3.74 \times 10^5$ and $E_{s_4} = 5.60 \times 10^5$.

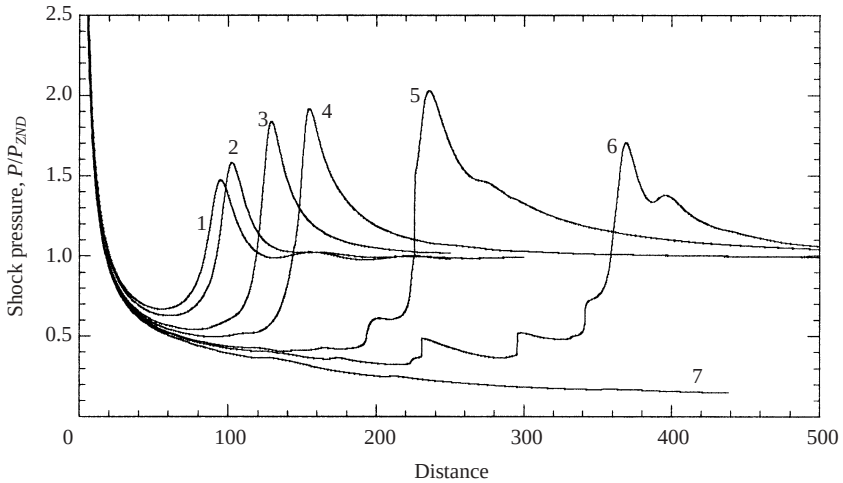


FIGURE 24. Leading shock pressure versus position for direct initiation using one-step kinetic rate law for $Q = 41.667$, $\gamma = 1.2$ and $E_a = 20$ for different initiation energies: $E_{s_1} = 3243$, $E_{s_2} = 3285$, $E_{s_3} = 3302$, $E_{s_4} = 3361$, $E_{s_5} = 3420$, $E_{s_6} = 3601$ and $E_{s_7} = 3724$.

& Quirk (1997) succeeded in obtaining a criterion for this limit, i.e. onset of the detonability limit occurs when the shock temperature drops to the chain-branching cross-over temperature. For the direct initiation of detonation, a well-defined value of the critical energy can also be obtained if the blast wave generated by the source energy never drops below the chain-branching cross-over temperature $T_B$. If the energy is insufficient and the blast drops below the chain-branching cross-over temperature $T_B$, then the chain-branching reaction is effectively being switched off. Since the chain-branching induction length is now much longer than the recombination-zone length, the rate of heat release is significantly reduced. In this case, the combustion front will no longer be able to couple with the leading shock and form a self-sustained detonation. From a purely chemical kinetic consideration, the following criterion for

defining the critical initiation energy can be obtained: *For successful initiation, the blast wave generated by the source must not drop below the chain-branching cross-over temperature before the onset of detonation occurs.*

Once the temperature drops below this limit, no initiation of detonation is possible. Thus, we see that the use of a three-step chain-branching reaction scheme has an advantage over the standard one-step Arrhenius kinetic model for the problem of direct initiation in that it can provide a 'cut-off' temperature and this leads to the possibility of obtaining a more well-defined value for the critical initiation energy.

## 5. General theories for direct initiation

In the past two decades, several theories have been developed to estimate the critical initiation energy for direct initiation of detonation from a point source. Because there is no clear definition for what value of the critical energy should be chosen when a single-step Arrhenius rate law is used, these theories for direct initiation cannot be verified numerically from previous studies. Hence, it appears worthwhile to examine the validity of these theories from the results of the present numerical simulations, where a different reaction mechanism is used.

### 5.1. *Dependence of critical energy on induction length*

A criterion for direct initiation was first proposed by Zel'dovich *et al.* (1957). For successful initiation, they stated that the blast radius should be on the order of the induction-zone thickness by the time the shock strength has decayed to the CJ value. From this argument, they demonstrated that the critical energy for direct initiation of spherical detonation must be proportional to the cube of the induction zone thickness, i.e. $\sim \Delta_{ind}^3$. Later, Lee (1977) extended the Zel'dovich *et al.*'s initiation criterion to other geometries in the form of $\sim \Delta_{ind}^{j+1}$, where $j = 0, 1, 2$ for planar, cylindrical and spherical geometries, respectively. In the past forty years, most of the initiation models have involved almost the same correlation between a characteristic chemical length and the critical initiation energy as described by Zel'dovich *et al.*'s model. Since Zel'dovich *et al.*'s criterion forms the base of many of these initiation models, it appears worthwhile to examine its validity for different geometries from the results of the present numerical simulations using a more detailed chemical kinetic model, where the critical energy can be clearly defined.

The critical initiation energies for different geometries calculated by numerical simulations are plotted versus the induction-zone length of the steady ZND detonation in figure 25. The corresponding induction-zone length for the detonability limit (above which no detonation can be formed) is also indicated in this figure. It is shown that the critical initiation energy correlates well with the induction zone length as predicted by Zel'dovich *et al.*'s theory. The linear, quadratic and cubic correlations (shown by the dashed lines in figure 25) between the critical initiation energy and the ZND induction-zone length for planar, cylindrical and spherical cases appear to be valid, especially for the case of a short induction zone, where the detonation is stable. For a long induction zone where the detonation is unstable, other effects such as curvature and non-steady expansion begin to influence the initiation process and the critical energy departs from the simple blast wave scaling law on which Zel'dovich *et al.*'s theory is based. For all three geometries, it is observed that there is a small deviation from Zel'dovich *et al.*'s criterion for a long induction zone. As mentioned previously, Zel'dovich *et al.*'s criterion simply relates the critical initiation energy with a chemical length scale, which does not include the effect of unsteadiness. Therefore, it is not

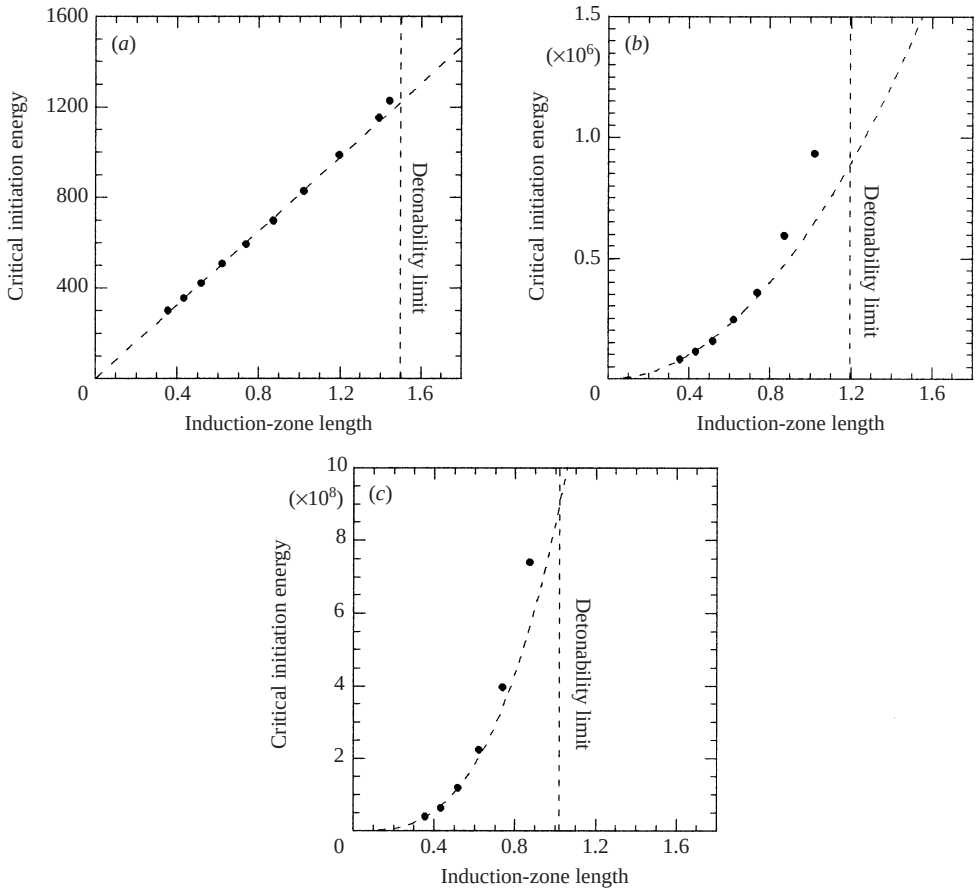


FIGURE 25. Variation of critical initiation energy with ZND induction-zone length for (*a*) planar $j = 0$, (*b*) cylindrical $j = 1$ and (*c*) spherical $j = 2$ geometries. The dashed lines show the correlation curve $\sim \Delta_{ind}^{j+1}$ for each geometry.

appropriate to simply use the induction-zone length for the very unsteady events in the initiation process. Furthermore, this deviation is more significant in cylindrical and spherical geometries because curvature appears to enhance the instability of the wave. Nevertheless, Zel'dovich *et al.*'s theory provides a means to estimate the correct order of magnitude of the critical initiation energy.

### 5.2. *Invariance of the critical explosion length* $R_o$

For direct initiation of detonation for different geometries, Lee (1977) has suggested that for a given combustible mixture, the critical explosion length $\tilde{R}_o$ is invariant with geometry and is defined as

$$\tilde{R}_o = \left(\frac{\tilde{E}_{spherical}}{\tilde{p}_o}\right)^{1/3} = \left(\frac{\tilde{E}_{cylindrical}}{\tilde{p}_o}\right)^{1/2} = \left(\frac{\tilde{E}_{planar}}{\tilde{p}_o}\right). \tag{5.1}$$

Consistent with the earlier normalization the explosion length is also normalized here by the reference length scale defined earlier (i.e. $R_o = \tilde{R}_o/\tilde{r}_c$). The explosion length $R_o$ represents a characteristic length of the source energy specific to the geometry and

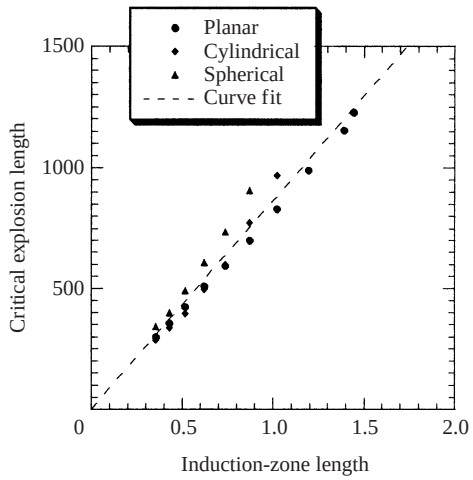


FIGURE 26. Invariance of explosion length $R_o$ for blast initiation for different geometries.

is the only length scale associated with strong blast decay. Recently, the explosion length concept has been verified experimentally by Radulescu, Higgins & Lee (2000). From the results of numerical simulations using the present three-step chemical model for different geometries, it is also possible to verify numerically the critical explosion length scaling law proposed by Lee (1977). To do this, the critical explosion lengths for direct initiation in planar, cylindrical and spherical detonations are plotted in figure 26. From this figure, it appears that the explosion length is essentially invariant for all the three geometries for the same mixture parameters, especially for those results corresponded to a stable detonation. Again, there is a small deviation for a long induction zone. As mentioned previously, this is due to the fact that the detonation becomes highly unstable for a long induction zone and the instability has a significant effect on the initiation process.

The invariance of the critical explosion length with geometry is quite useful in practice because we can predict the critical initiation energy for different geometries if it is known for one geometry. For example with the critical value of the explosion length known, then the critical initiation energy, energy per unit length and energy per unit area for the three basic geometries could be determined, i.e.

$$R_o = \frac{E_{spherical}}{E_{cylindrical}} = \frac{E_{cylindrical}}{E_{planar}}. \tag{5.2}$$

Since the critical initiation energy is linked to the chemical length scale $\Delta_{ind}$ of the detonation, i.e. $\sim \Delta_{ind.}^{j+1}$, and from the explosion length invariance principle for different geometries, we could expect that the critical explosion length should also scale with the chemical length of the detonation, i.e. $R_o \sim \Delta_{ind}$. In the present numerical study, the explosion length $R_o$ under critical conditions is found to be of the order of $R_o \sim 864\Delta_{ind}$. Using the standard correlation between the cell size and induction length $\Delta_{ind}$ of the form $\lambda \sim 30\Delta_{ind}$ (Westbrook & Urtiew 1982), the explosion length $R_o$ under critical conditions can be roughly correlated with the cell size. In the present study, we obtain $R_o$ of the order of $\sim 29\lambda$, which is close to some experimental results, i.e. $R_o$ varies from $17\lambda$ to $24\lambda$ for typical hydrocarbon–air mixtures found by Benedick *et al.* (1985) and $R_o \sim 33\lambda$ in the recent study by Radulescu *et al.* (2000).

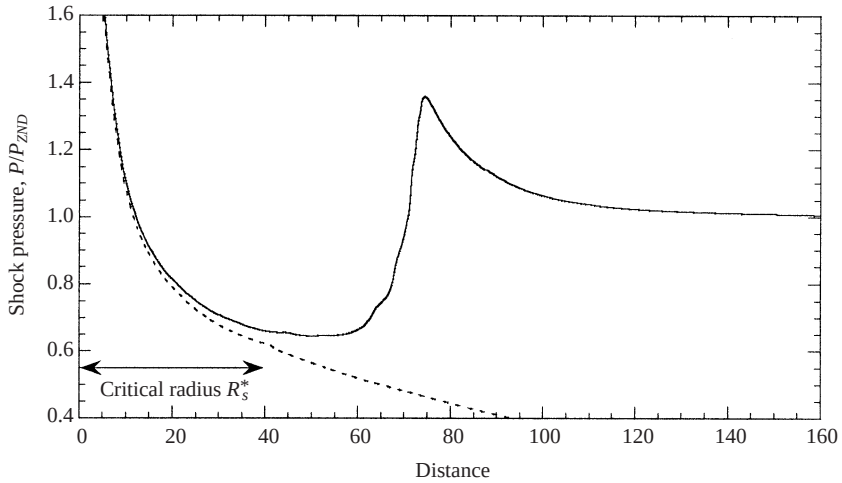


FIGURE 27. Definition of critical radius $R_s^*$ from the results of numerical simulations.

### 5.3. *Critical kernel radius $R_s^*$ for direct initiation*

The detonation kernel theory of Lee & Ramamurthi (1976) states that there exists a critical size of detonation kernel for direct initiation. The size of the detonation kernel corresponds to the shock radius $R_s^*$ at which the shock wave has decayed to some critical Mach number $M_s^*$ before it re-accelerates back to a CJ detonation. The appropriate choice of critical Mach number $M_s^*$ should reflect the critical shock strength below which any detonation would fail. The shock strength prior to the onset of detonation, during the so-called quasi-steady period, appears to be an appropriate value for the critical Mach number $M_s^*$. Experimentally, the shock strength during the quasi-steady period is observed to be close to half the CJ detonation speed. The half-CJ value is generally accepted for the critical Mach number $M_s^*$ and is used in many initiation models (Lee 1977). However, this half-CJ value is only a general estimate from experimental observations and may be incorrect for different explosive mixtures. The present study suggests that the choice of critical Mach number should take into account the chemistry. In the previous section, it is shown that if the blast wave generated by an initial point source drops below the chain-branching cross-over temperature $T_B$, initiation of detonation fails. Therefore, the shock temperature during the quasi-steady period should be close to this chain-branching cross-over temperature $T_B$. Hence, the shock strength to this temperature limit should be a more suitable choice of the critical Mach number $M_s^*$, which corresponds to the shock strength very near the auto-ignition limit of a combustible mixture. Depending on the value of the chain-branching cross-over temperature $T_B$, the critical Mach number ranges from $0.5M_{CJ}$ to $0.9M_{CJ}$.

In the numerical results, the critical radius $R_s^*$ is defined as the radius before the re-acceleration of the shock to detonation at the critical condition, as shown in figure 27. The approximate values of critical radius $R_s^*$ from the present numerical simulations for different mixtures are given in table 2. Conventionally, the critical kernel $R_s^*$ at which the onset of detonation occurs is usually correlated to the cell size of the mixture, which is the most important dynamic parameter of gaseous detonation. Estimates of the critical kernel radius for initiation vary widely in the literature. Table 3 shows some experimental results of critical radius for each geometry for

| Induction length $\Delta_{ind}$ | $R^*_{planar}/\Delta_I$ | $R^*_{cylindrical}/\Delta_I$ | $R^*_{spherical}/\Delta_I$ |
|---|---|---|---|
| 0.353 | 90.74 | 269.39 | 411.18 |
| 0.431 | 88.11 | 255.05 | 417.36 |
| 0.517 | 81.21 | 212.70 | 386.73 |
| 0.619 | 74.31 | 206.80 | 355.43 |
| 0.737 | 70.59 | 190.04 | 352.93 |
| 0.870 | 68.94 | 201.07 | 344.69 |
| 1.021 | 68.54 | 215.42 | — |
| 1.194 | 67.01 | — | — |
| 1.390 | 66.20 | — | — |
| 1.443 | 67.22 | — | — |

TABLE 2. Results of critical radius $R^*_s$ for direct initiation of detonation obtained from the present numerical simulations.

| | $R^*_s$ |
|---|---|
| Spherical | $\approx 10 - 13\lambda$ (Bull *et al.* 1978) |
| Cylindrical | $\approx 4 - 8\lambda$ (Radulescu *et al.* 2000) |
| Planar | less than $3\lambda$ (Benedick 1979) |

TABLE 3. Results of critical radius $R^*_s$ for direct initiation obtained from some experiments.

typical hydrocarbon combustible mixtures. For qualitative comparison, the standard correlation between the cell size and induction length $\Delta_{ind}$ of the form $\lambda \sim 30\Delta_{ind}$ is used once again. Using this correlation, we obtain approximately the values of critical radius from the results of the present numerical simulations in term of cell size, i.e. $R^*_{planar} \sim 2\lambda$, $R^*_{cylindrical} \sim 7\lambda$ and $R^*_{spherical} \sim 12\lambda$. These are in accordance with the experimental results shown in table 3.

## 6. Conclusion

The problem of direct initiation of detonation using a multi-step chemical kinetic model has been investigated here. The three-step chemical kinetic scheme used for this study represents the simplest mechanism capable of reproducing some essential features of a chain-branching reaction. Due to the different mechanism of a chain-branching chemical reaction compared to a one-step global reaction, some qualitative differences between these two chemical kinetic models can be observed for the initiation and propagation of the detonation. This study demonstrates that using a more detailed chemical kinetic model could eliminate some of the difficulties in a one-step Arrhenius chemical approximation and it was able to more accurately reproduce the qualitative aspects of the direct initiation of detonation. The multi-step chemical kinetic scheme can provide a chemical switch-off mechanism that causes detonation failure to occur, which cannot be described by the one-step Arrhenius reaction model. This permits a more clear value for the critical initiation energy to be determined. From the point of view of chemical kinetics, a criterion for defining a critical initiation energy can also be obtained, based on the blast wave generated by the source not decaying below the chain-branching cross-over temperature before the onset of detonation occurs. Below this temperature limit, chain-branching reactions become ineffective, resulting in a sudden decrease in the global reaction rate and causing a quenching of energy release and a failure to initiate.

Due to the difficulty in determining a well-defined value of the critical energy when a single-step Arrhenius rate law is used, most of the existing theories on direct initiation cannot be verified numerically. In the present study where a three-step chemistry model that describes branched-chain processes is used and a clear cut-off value of critical energy can be reasonably approximated, some of these theories have been verified. The numerical results show that the detonation instability plays an important role in the initiation process. For a highly unstable mixture, results deviate from those obtained by previous theories for direct initiation. Since most of these existing initiation models are based on the blast wave theory, they do not include a parameter to model the detonation instability. This study suggests that the ratio $\delta$ between the induction- and reaction-zone length may be a useful parameter to include in the formulation of a theory for direct initiation to take into account the effect of detonation instability. Regardless of the chemical reaction mechanism, this ratio $\delta$ is shown to control the detonation propagation. In addition, it is thought to govern the mechanism of the amplification process for initiation near the critical regime. For this reason, a multi-step chemical kinetic model is certainly required to investigate in more detail the effect of this ratio $\delta$ because it allows the independent variation of the induction and reaction length scales, which cannot be achieved by a single-step Arrhenius chemical kinetics. This will permit us in the future to perform a parametric study of these two length scales numerically and contribute to the development of a more rigorous theory for direct initiation.

In conclusion, this paper suggests that a multi-step chemical kinetic model, for example similar to the one employed in the present study, should be considered for a more comprehensive study of the direct initiation of detonation.

The authors are grateful to Dr Kiumars Mazaheri and Dr Randy Chue for their valuable help on the numerics, and would also like to acknowledge the useful comments made by the referees. H. D. Ng is supported by a Natural Science and Engineering Research Council of Canada (NSERC) scholarship.

## REFERENCES

Bach, G. G., Knystautas, R. & Lee, J. H. S. 1969 Direct initiation of spherical detonations in gaseous explosives. In *Proc. 12th Symp.* (*Intl*) *on Combustion*, pp. 853–864. The Combustion Institute.

Benedick, W. B. 1979 High-explosive initiation of methane-air detonations. *Combust. Flame* **35**, 87–91.

Benedick, W. B., Guirao, C., Knystautas, R. & Lee, J. H. S. 1985 Critical charge for the direct initiation of detonation in gaseous fuel-air mixtures. *Prog. Astro. Aero.* **106**, 181–202.

Berger, M. J. & Collela, P. 1989 Local adaptive mesh refinement for shock hydrodynamics. *J. Comput. Phys.* **82**, 64–84.

Borisov, A. A., Zamanskii, V. M. & Lisyanskii, V. V. 1987 Heat evolution kinetics in high-temperature ignition of hydrocarbon/air or oxygen mixtures. *Prog. Astro. Aero.* **114**, 124–139.

Bourlioux, A. 1991 Numerical studies of unstable detonations. PhD thesis, Princeton University, Princeton, New Jersey, USA.

Bourlioux, A., Majda, A. J. & Roytburd, V. 1991 Theoretical and numerical structure for unstable one-dimensional detonations. *SIAM J. Appl. Maths* **51**, 303–343.

Bull, D. C., Elsworth, J. E. & Hooper, G. 1978 Initiation of spherical detonation in hydrocarbon/air mixtures. *Acta Astro.* **5**, 997–1008.

Chern, I. L. & Colella, P. 1987 A conservative front tracking method of hyperbolic conservation laws. *Lawrence Livermore National Laboratories Rep. No.* UCRL-97200.

Clarke, J. F., Kassoy, D. R., Meharzi, N. E., Riley, N. & Vasantha, R. 1990 On the evolution of plane detonations. *Proc. R. Soc. Lond.* A **429**, 259–283.

Clarke, J. F., Kassoy, D. R. & Riley, N. 1986 On the direct initiation of a plane detonation wave. *Proc. R. Soc. Lond.* A **408**, 129–148.

Colella, P. & Woodward, P. R. 1984 The piecewise parabolic method (PPM) for gas dynamical simulations. *J. Comput. Phys.* **54**, 174–201.

Dionne, J.-P. 2000 Numerical study of the propagation of non-ideal detonations. PhD thesis, McGill University, Montreal, Canada.

Dold, J. W. & Kapila, A. K. 1991 Comparison between shock initiations of detonation using thermally-sensitive and chain-branching chemical models. *Combust. Flame* **85**, 185–194.

Eckett, C. A., Quirk, J. J. & Shepherd, J. E. 2000 The role of unsteadiness in direct initiation of gaseous detonations. *J. Fluid Mech.* **421**, 147–183.

Erpenbeck, J. J. 1964 Stability of idealized one-reaction detonations. *Phys. Fluids* **7**, 684–696.

Fickett, W. & Davis, W. C. 1979 *Detonation.* University of California Press.

Fickett, W. & Wood, W. W. 1966 Flow calculation for pulsating one-dimensional detonations. *Phys. Fluids* **9**, 903–916.

He, L. 1996 Theoretical determination of the critical conditions for the direct initiation of detonations in hydrogen-oxygen mixtures. *Combust. Flame* **104**, 401–418.

He, L. & Clavin, P. 1994 On the direct initiation of gaseous detonation by an energy source. *J. Fluid Mech.* **277**, 227–248.

He, L. & Lee, J. H. S. 1995 The dynamic limit of one-dimensional detonations. *Phys. Fluids* **7**, 1151–1158.

Korobeinikov, V. P. 1991 *Problems of Point-Blast Theory.* American Institute of Physics.

Lee, H. I. & Stewart, D. S. 1990 Calculation of linear detonation instability: One-dimensional instability of plane detonation. *J. Fluid Mech.* **216**, 103–132.

Lee, J. H. S. 1977 Initiation of gaseous detonation. *Annu. Rev. Phys. Chem.* **28**, 75–104.

Lee, J. H. S. & Higgins, A. J. 1999 Comments on criteria for direct initiation of detonations. *Phil. Trans. R. Soc. Lond.* A **357**, 3503–3521.

Lee, J. H. S. & Moen, I. O. 1980 The mechanism of transition from deflagration to detonation in vapor cloud explosions. *Prog. Energy Combust. Sci.* **6**, 359–389.

Lee, J. H. S. & Ramamurthi, K. 1976 On the concept of the critical size of a detonation Kernel. *Combust. Flame* **27**, 331–440.

Mazaheri, B. K. 1997 Mechanism of the onset of detonation in blast initiation. PhD thesis, McGill University, Montreal, Canada.

von Neumann, J. 1942 Theory of detonation wave. OSRD 549; reprinted in *John von Neumann: Collected Works*, Vol. 6, Macmillan 1963.

Radulescu, M. I., Higgins, A. J. & Lee, J. H. S. 2000 On the explosion length invariance in direct initiation of detonation. In *Proc. 28th Symp. (Intl) on Combustion,* pp. 637–644. The Combustion Institute.

Sánchez, A. L., Carretero, M., Clavin, P. & Williams, F. A. 2001 One-dimensional overdriven detonations with branched-chain kinetics. *Phys. Fluids* **13**, 776–792.

Sedov, L. I. 1959 *Similarity and Dimensional Method in Mechanics*, 4th edn. Academic.

Sharpe, G. J. 1997 Linear stability of idealized detonations. *Proc. R. Soc. Lond.* A **453**, 2603–2625.

Sharpe, G. J. 1999 Linear stability of pathological detonations. *J. Fluid Mech.* **401**, 311–338.

Sharpe, G. J. & Falle, S. A. E. G. 1999 One-dimensional numerical simulations of idealized detonations. *Proc. R. Soc. Lond.* A **455**, 1203–1214.

Sharpe, G. J. & Falle, S. A. E. G. 2000 One-dimensional nonlinear stability of pathological detonations. *J. Fluid Mech.* **414**, 339–366.

Short, M. & Dold, J. W. 1996 Multi-dimensional linear stability of a detonation wave with a model three-step chain-branching reaction. *Math. Comput. Model.* **24**, 115–123.

Short, M., Kapila, A. K. & Quirk, J. J. 1999 The chemical-gas dynamic mechanisms of pulsating detonation wave instability. *Phil. Trans. R. Soc. Lond.* A **357**, 3621–3637.

Short, M. & Quirk, J. J. 1997 On the nonlinear stability and detonability limit of a detonation wave for a model three-step chain-branching reaction. *J. Fluid Mech.* **339**, 89–119.

Taylor, S. G. 1950 The formation of blast wave by a very intense explosion, I. Theoretical discussion. *Proc. R. Soc. Lond.* A **201**, 159–174.

Westbrook, C. K. & Urtiew, P. A. 1982 Chemical kinetic prediction of critical parameters in gaseous detonations. In *Proc. 19th Symp.* (*Intl*) *on Combustion*, pp. 615–623. The Combustion Institute.

Zel'dovich, Ya. B., Kogarko, S. M. & Simonov, N. N. 1957 An experimental investigation of spherical detonation in gases. *Sov. Phys. Tech. Phys.* **1**, 1689–1713.